

# Revisiting the Thickness of the Air–Water Interface from Two Extremes of Interface Hydrogen Bond Dynamics

Gang Huang and Jie Huang\*



Cite This: *J. Chem. Theory Comput.* 2024, 20, 9107–9115



Read Online

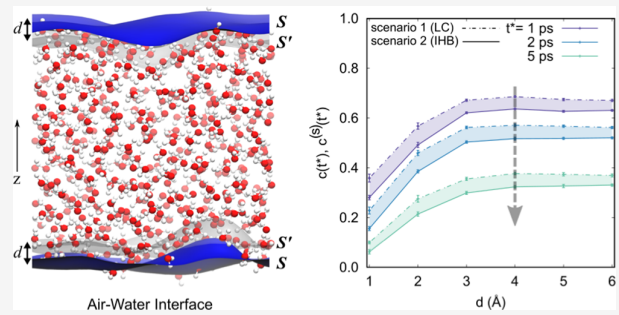
ACCESS |

Metrics & More

Article Recommendations

Supporting Information

**ABSTRACT:** The air–water interface plays a crucial role in many aspects of science because of its unique properties, such as a two-dimensional hydrogen bond (HB) network and completely different HB dynamics compared to bulk water. However, accurately determining the boundary of interfacial and bulk water, that is, the thickness of the air–water interface, still challenges experimentalists. Various simulation-based methods have been developed to estimate the thickness, converging on a range of approximately 3–10 Å. In this study, we introduce a novel approach, grounded in density functional theory-based molecular dynamics and deep potential molecular dynamics simulations, to measure the air–water interface thickness, offering a different perspective based on prior research. To capture realistic HB dynamics in the air–water interface, two extreme scenarios of the interface HB dynamics are obtained: one underestimates the interface HB dynamics, while the other overestimates it. Surprisingly, our results suggest that the interface HB dynamics in both scenarios converges as the thickness of the air–water interface increases to 4 Å. This convergence point, indicative of the realistic interface thickness, is also validated by our calculation of anisotropic decay of OH stretch and the free OH dynamics at the air–water interface.



## 1. INTRODUCTION

The air–water interface has been the subject of extensive study due to its ubiquity in nature and its unusual macroscopic properties as a model system for aqueous hydrophobic interfaces.<sup>1–16</sup> It is widely accepted that water molecules behave in a completely different manner at the interface than in the bulk phase.<sup>17–19</sup>

Advances in the study of hydrogen bond (HB) dynamics at the air–water interface have been significant. Liu et al.<sup>20</sup> used molecular dynamics (MD) simulations to demonstrate faster HB breaking and forming at the interface than bulk water, attributed to quicker translational diffusion. From sum frequency generation (SFG) vibrational spectroscopy, Gan et al.<sup>21</sup> found that at the air–water interface, singly hydrogen (H)-bonded water molecules align almost parallel to the interface with limited orientational variation, while doubly H-bonded donor molecules orient their dipole vectors away from the liquid phase, highlighting diverse behaviors among interfacial water molecules. Almost concurrently, through time-resolved SFG vibrational spectroscopy, McGuire and Shen<sup>22</sup> observed ultrafast vibrational dynamics at the interface, noting that the relaxation behaviors of interfacially bonded OH stretch modes on subpicosecond time scales were akin to those in bulk water, encompassing spectral diffusion, vibrational relaxation, and thermalization. Pioneering work by Tahara's group,<sup>23,24</sup> which presented the first two-dimensional heterodyne-detected vibrational SFG (2D HD-VSFG) spectra of the

OH stretch region at the interface, highlighted diverse behaviors among interfacial HB OH groups. Subsequent studies, including those by Jeon et al.<sup>25</sup> and Ojha and Kühne,<sup>26</sup> have used MD and ab initio MD (AIMD) simulations to explore the structure and dynamics of interfacial water, uncovering weaker H-bonds and faster vibrational spectral dynamics of free OH groups compared to H-bonded OH groups at the interface. These collective insights enhance our understanding of the vibrational energy relaxation, HB dynamics, and interactions of water molecules at the air–water interface. Building upon this knowledge of interfacial behavior, significant efforts have also been directed toward quantifying the physical characteristics of the interface, including its thickness, which plays a crucial role in understanding its molecular interactions and behavior.

The air–water interface thickness has been measured via ellipsometry,<sup>27–29</sup> relative permittivity measurements,<sup>30</sup> X-ray reflectivity,<sup>31,32</sup> SFG spectroscopy,<sup>23,33–41</sup> classical MD simulations<sup>20,42–51</sup> and the AIMD simulations<sup>25,41,52–55</sup> to mention

Received: April 6, 2024

Revised: September 15, 2024

Accepted: September 24, 2024

Published: October 4, 2024



ACS Publications

© 2024 American Chemical Society

9107

<https://doi.org/10.1021/acs.jctc.4c00457>

*J. Chem. Theory Comput.* 2024, 20, 9107–9115

just a few. There is a consensus that the thickness of the air–water interface is about 3–10 Å.<sup>42,43,45–47,S2,S4,S6–S9</sup> Nonetheless, accurately determining the thickness remains experimentally challenging. The MD and Monte Carlo (MC) simulations of the air–water interface yield molecular-level information not readily available in experiments. These simulations, which utilize various intermolecular potential functions, have played a crucial role in estimating the thickness.<sup>41,60–67</sup> Additionally, density functional theory-based MD (DFTMD) simulations<sup>S2,68–73</sup> also offer a predictive platform for understanding density profiles and determining the thickness of the air–liquid interfaces.<sup>S2,S4,74,75</sup>

Nevertheless, DFTMD simulations are constrained by limitations in time and the number of molecules they can model. Traditional force field approaches, however, often lack the accuracy required to describe complex interface systems.<sup>76</sup> Recently, deep potential molecular dynamics (DeePMD) simulations based on machine learning potential (MLPs) have emerged as a promising alternative, offering a solution to the accuracy-versus-efficiency dilemma in molecular simulations.<sup>77</sup> One of the most accurate MLPs for water is MB-pol, which accurately reproduces many properties of water across the phase diagram.<sup>78–82</sup> Moreover, MB-pol has been used to obtain the VSFG and surface tension of air–water interface, demonstrating excellent agreement between theoretical predictions and experimental measurements.<sup>83</sup>

Inspired by the above experimental and simulation results, and with the motivation of capturing realistic HB dynamics at interfaces, we have designed an approach based on two extreme scenarios of interface HB dynamics by utilizing the trajectories of DFTMD and DeePMD simulations based on MB-pol. In the first scenario, for the set of molecules located in the interface layer at given sampling times, we use the Luzar-Chandler (LC) HB population operator<sup>84</sup> to obtain the HB dynamics of these interface molecules. In the second scenario, taking inspiration from Luzar and Chandler's HB population and the characteristic function introduced by Giberti and Hassanali,<sup>85</sup> we have developed an interface HB (IHB) population operator. This operator aims to provide a refined understanding of HB dynamics specifically at the interface.

The Luzar-Chandler HB population is utilized to describe whether a pair of labeled molecules form H-bonds. And the characteristic function developed by Giberti and Hassanali describes whether a specific molecule belongs to the interface region. Therefore, our newly defined interface HB population can describe whether a labeled pair of molecules is within the interface *and* connected by H-bonds at any given moment. This dual condition provides a more detailed understanding of interfacial HB dynamics.

Due to the thermal motion of water molecules, two scenarios may occur. In the first scenario, the water molecules under observation might transition into the bulk phase. In the second scenario, if a water molecule resides in the interface region *and* its H-bonded partner moves outside the interface area, then such a pair of molecules will no longer be of concern. Based on the study of interfacial water dynamics by Liu et al.,<sup>20</sup> Gan et al.,<sup>21</sup> Singh et al.,<sup>23</sup> and Jeon et al.,<sup>25</sup> as well as the investigation into the time-dependent spectral evolution of H-bonded and free water molecules by Ojha and Kühne,<sup>26</sup> our approach indicates that the HB dynamics derived from the first scenario will be slower than the genuine interfacial HB dynamics. Conversely, the one obtained from the second scenario will exhibit faster dynamics than the genuine one.

Building upon the foundation laid by methods reliant on the density criterion,<sup>1,63–66,S6–S9</sup> our approach introduces an alternative way of determining interface thickness through the analysis of the convergence of interfacial HB dynamics properties. This approach effectively bypasses the necessity of accounting for liquid density. As such, it offers another perspective for measuring the thickness of the air–water interface. Furthermore, the principles underlying our approach hold potential for application to a broader range of systems, such as solution interfaces and ion shells, offering a flexible tool for interface studies.

## 2. METHODS

Due to molecular motions, the identity of molecules at the interface changes with time, and generally useful procedures for identifying interfaces must accommodate these motions. The air–water boundary is modeled with the Willard-Chandler instantaneous surface.<sup>48,75,91</sup> Figure 1 illustrates the obtained interfaces for one configuration of a slab of water.

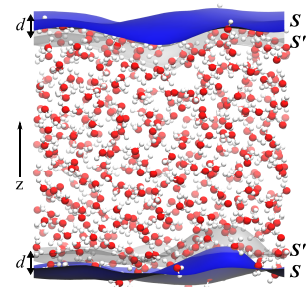


**Figure 1.** Slab of water containing 512 water molecules with the instantaneous surface  $S$  represented as a blue mesh on the upper and lower phase boundary. Gray surface, which represents an imaginary interface  $S'$ , is obtained by translating the surface to the inside of the system along the normal ( $z$ -axis) by distance  $d$ . This variable  $d$  is then utilized to measure the thickness of the air–water interface.

For the slab in the cuboid simulation box, an imaginary surface  $S'(t)$  is obtained by translating the surface  $S(t)$  along the system's normal (into bulk) to a distance  $d$ . The region between the two surfaces  $S(t)$  and  $S'(t)$  is defined as the air–water interface. Below we will combine two extreme scenarios to investigate the HB dynamics at the instantaneous air–water interface.

**2.1. Scenario 1: HB Dynamics Based on the Luzar-Chandler HB Population.** As the first scenario we use the Luzar-Chandler HB population and employ a technique that samples water molecules right at the instantaneous interface for certain sampling time points. In Scenario 1, we divide the simulation trajectory into multiple subtrajectories of length  $t_{\text{traj}}$ . Within these subtrajectories, the majority of water molecules exhibit thermal fluctuations near their equilibrium positions. Meanwhile, a select group of molecules initially at the interface may transition into the bulk phase at a later time. Due to the inclusion of H-bonds in the bulk phase, this scenario tends to *underestimate* the breaking rate of the H-bonds at the interface. In Section 3 of this paper, we will see this result, combined with the outcome from Scenario 2, can be used to estimate the thickness of the air–water interface. This method includes three steps as follows:

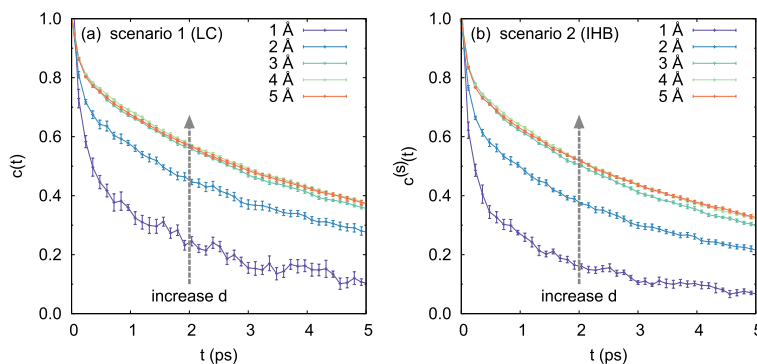


**Figure 2.** Autocorrelation functions  $c(t)$  and  $c^{(s)}(t)$  for interface H-bonds with different thickness  $d$  for (a) Scenario 1 (LC) and (b) Scenario 2 (IHB). Two notable features emerge: (i) As  $d$  increases, both  $c(t)$  and  $c^{(s)}(t)$  eventually approach a stable function. (ii) Decay rate of  $c^{(s)}(t)$  in Scenario 2 is greater than that of  $c(t)$  in Scenario 1. This behavior is visually represented by two dashed directed line segments, positioned identically to the graphs. Functions  $c(t)$  and  $c^{(s)}(t)$  on a log–log scale are also plotted in Supporting Information.

*a. Subtrajectories.* Subtrajectories with a specific length of time,  $t_{\text{trap}}$ , are selected. In this work,  $t_{\text{trap}}$  is set to be 40 (ps), which is long enough to observe HB dynamics but short enough that not all the molecules complete their transition across the interface.<sup>92</sup>

*b. Sampling.* For each time step, we identify a pair of the air–water interfaces of a specified thickness  $d$  as shown in Figure 1. At evenly spaced moments within  $t_{\text{trap}}$ , we select the water molecules within the interfaces. For the union of the interfacial water molecules picked at all these time moments, the Luzar-Chandler HB population-based correlation functions<sup>84</sup> across the subtrajectory are calculated.

*c. Statistics.* The average correlation functions across all subtrajectories are calculated.

In this scenario, the computational procedure for calculating HB dynamics follows the same methodology as that used in works based on the Luzar-Chandler's method (LC method).<sup>20,93,94</sup> For details on this method, please refer to the Supporting Information.

**2.2. Scenario 2: HB Dynamics Based on Interface HB Population.** To capture the other extreme of interfacial HB dynamics, after determining the instantaneous interface, we introduce an interface HB population operator  $h^{(s)}[\mathbf{r}(t)]$  as follows: It has a value of 1 when a tagged molecular pair  $i, j$  are H-bonded and both molecules are at the interface with a thickness  $d$ , and 0 otherwise:

$$h^{(s)}[\mathbf{r}(t)] = \begin{cases} 1 & \mathbf{r}_i \in \mathcal{I}(d; t), \mathbf{r}_j \in \mathcal{I}(d; t), \\ & j \in \mathcal{B}_i(t); \\ 0 & \text{otherwise} \end{cases} \quad (1)$$

where  $\mathbf{r}(t)$  is the configuration of the system at time  $t$ ,  $\mathbf{r}_i$  is the position coordinate of the oxygen atom in the  $i$ th water molecule,  $\mathcal{B}_i(t)$  denotes the set of water molecules that are H-bonded with molecule  $i$  at time  $t$ , and  $\mathcal{I}(d; t)$  is the instantaneous interface layer with thickness  $d$  at time  $t$ . The definition of  $h^{(s)}$  combines the Luzar-Chandler's HB population<sup>84,95</sup>  $h$  and the characteristic function introduced by Giberti and Hassanali.<sup>85</sup> Then the correlation function  $c^{(s)}(t)$  that describes the fluctuation of H-bonds at the interface:

$$c^{(s)}(t) = \frac{\langle h^{(s)}(0)h^{(s)}(t) \rangle}{\langle h^{(s)} \rangle} \quad (2)$$

can be obtained. Similar to functions  $n(t)$  and  $k(t)$  in ref 84 (eqs 1 and 2 in Supporting Information), the corresponding correlation function

$$n^{(s)}(t) = \frac{\langle h^{(s)}(0)[1 - h^{(s)}(t)]h^{(d,s)} \rangle}{\langle h^{(s)} \rangle} \quad (3)$$

and interface reactive flux function

$$k^{(s)}(t) = -\frac{dc^{(s)}(t)}{dt} \quad (4)$$

are obtained. The  $h^{(d,s)}(t)$  is 1 when a tagged pair of water molecules  $i, j$  is at the interface and the interoxygen distance between the two molecules is less than the cutoff radius  $r_{\text{OO}}^c$  at time  $t$ , and 0 otherwise, i.e.,

$$h^{(d,s)}[\mathbf{r}(t)] = \begin{cases} 1 & \mathbf{r}_i \in \mathcal{I}(d; t), \mathbf{r}_j \in \mathcal{I}(d; t), \\ & |\mathbf{r}_i - \mathbf{r}_j| < r_{\text{OO}}^c; \\ 0 & \text{otherwise.} \end{cases} \quad (5)$$

Therefore,  $n^{(s)}(t)$  represents the probability at time  $t$  that a tagged pair of initially H-bonded water molecules at the interface are unbonded but remain at the interface and separated by less than  $r_{\text{OO}}^c$ ;  $k^{(s)}(t)$  measures the effective decay rate of H-bonds at the interface. The functions defined in eqs 2–4 are used to determine the reaction rate constants of breaking and reforming and the lifetimes of H-bonds at the interface by<sup>73,84</sup>

$$k^{(s)}(t) = kc^{(s)}(t) - k'n^{(s)}(t)$$

In this IHB scenario, choosing the water molecules and H-bonds at the interface is accurate. However, for some special H-bonds, if it connects such two water molecules, one is at the interface and the other is in the bulk phase, the HB breaking reaction rate of such H-bonds will be increased. Therefore, in contrast to the LC method used in Scenario 1, the IHB method used in this scenario overestimates the HB breaking rate constant.

The actual HB dynamics at the interface are expected to lie between the results obtained by the LC method and the IHB

method. Consequently, by integrating these two scenarios, we can achieve a more precise characterization of HB dynamics at the interface.

### 3. RESULTS AND DISCUSSIONS

In this section, we apply our two-extreme approach to two system properties: HB population autocorrelation functions and HB reaction rate constants. We then determine the thickness of the air–water interface based on each of these properties. The computational details for DFTMD and DeePMD simulations are available in the [Supporting Information](#). The results discussed in the following sections are derived from the trajectory data of the system containing 512 water molecules, modeled by MB-pol potential. Similar analyses for DFTMD simulations with 128 water molecules, and other system sizes in DeePMD simulations using MB-pol, are also provided in the [Supporting Information](#). The finite size effects of the main properties discussed in this article are also analyzed in [Supporting Information](#).

**3.1. HB Population Autocorrelation Functions.** Figure 2 illustrates the dynamic evolution of  $c(t)$  and  $c^{(s)}(t)$  for various values of distance  $d$ . When  $d$  is 4 Å or greater,  $c(t)$  and  $c^{(s)}(t)$  become largely invariant to further increases in  $d$ . This indicates that one can determine the thickness of the interface under different conditions by examining how the correlation function depends on distance  $d$ . Analysis of both scenarios reveals that the decay rate of the correlation function  $c^{(s)}(t)$  in Scenario 2 (IHB) surpasses that in Scenario 1 (LC).

Figure 3 displays the  $d$ -dependence of the correlation functions at three reference time points  $t^* = 1, 2, 5$  (ps). This

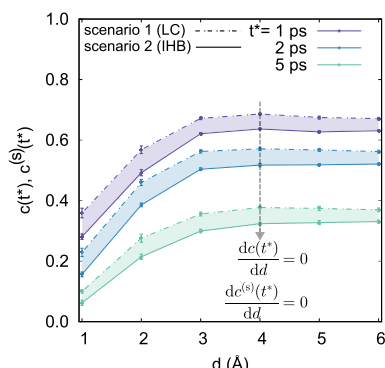


**Figure 3.** Dependence of the correlation functions on the distance  $d$  at three reference time points  $t^* = 1, 2, 5$  (ps) provides key insights into the dynamics of the air–water interface: (i) As  $d$  increases, both  $c(t^*)$  and  $c^{(s)}(t^*)$  exhibit an upward trend, with their rates of change gradually approaching 0. (ii) At each  $t^*$ ,  $c(t)$  is consistently slightly larger than  $c^{(s)}(t)$  for the same  $d$ . (iii) Air–water interface thickness  $d_f = 4$  Å is determined from the  $d$ -dependence of  $c(t^*)$  and  $c^{(s)}(t^*)$ , as calculated using the LC method (dot-dashed lines) and the IHB method (solid lines), respectively.

figure provides a different perspective on  $d$ -dependence: by selecting three reference time intervals on the  $t$ -axis in Figure 2, the values of the correlation functions,  $c(t)$  and  $c^{(s)}(t)$ , at these time intervals for each  $d$  were recorded. Comparing  $c(t)$  and  $c^{(s)}(t)$  in Figure 3,  $c(t)$  in Scenario 1 is always slightly larger than  $c^{(s)}(t)$  in Scenario 2 for the same  $d$ .

In Figure 3, both  $c(t^*)$  and  $c^{(s)}(t^*)$  increase as  $d$  increases, eventually reaching a point where their change rates approach

0 for sufficiently large values of  $d$ . Since  $c(t)$  and  $c^{(s)}(t)$  serve as the upper and lower bounds of the real interface correlation function  $c^r(t^*)$  respectively, it logically follows that the  $d$ -dependence of  $c^r(t^*)$  exhibits the same trend. Consequently, we arrive at the equations  $dc/dd = 0$  for  $c(t^*)$  and  $c^{(s)}(t^*)$  with respect to  $d$ . Solving for  $C = c(t^*)$  and  $C = c^{(s)}(t^*)$  yields solutions  $d_{f1}$  and  $d_{f2}$  respectively. Here  $d_{f1}$  and  $d_{f2}$  represent the thickness of the air–water interface as determined by the LC method and the IHB method, respectively. The average value  $d_f = (d_{f1} + d_{f2})/2$  is then obtained as the thickness of the interface for a given  $t^*$ .

The correlations  $c(t^*)$  and  $c^{(s)}(t^*)$  respectively describe the relaxation characteristics of HB dynamics within the air–water interface. For both the LC and IHB methods, the values of  $c(t^*)$  and  $c^{(s)}(t^*)$  cease to change significantly when  $d$  reaches 4 Å, i.e.,  $d_{f1} \approx d_{f2} = 4$  Å. Thus, we determine the thickness of the air–water interface in the simulations to be  $d_f = 4$  Å.

**3.2. HB Reaction Rate Constants.** We further examined how the reaction rate constants of H-bonds at the air–water interface vary with  $d$ . For further details regarding the HB reaction rate constants, please refer to Section 2 in Supporting Information.

In Figure 4, we compare the breaking HB reaction rate constants,<sup>84,93</sup>  $k_{LC}$  and  $k_{IHB}$ , obtained by the LC and IHB

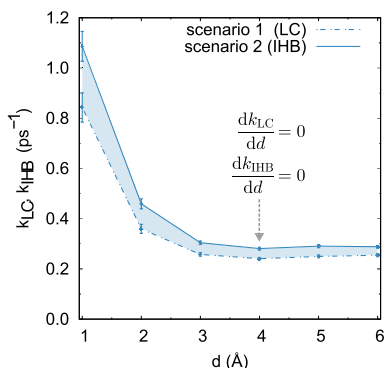


**Figure 4.** Breaking HB reaction rate constants  $k_{LC}$  and  $k_{IHB}$  for the air–water interface simulated with 512 water molecules, obtained by the LC and IHB methods, respectively. (i) Both constants,  $k_{LC}$  and  $k_{IHB}$ , decrease monotonically to the HB breaking rate  $k_{bulk}$  for the bulk water as  $d$  increases. (ii)  $k_{LC}$  is always smaller than  $k_{IHB}$  for the same  $d$ . (iii) Thickness  $d_f = 4$  Å of the air–water interface is obtained from the  $d$ -dependence of the rate constant  $k_{LC}$  and  $k_{IHB}$ , obtained by the LC method and the IHB method, respectively. (Consistent results for systems with 125 and 216 water molecules, please refer to the [Supporting Information](#)).

methods, respectively. We found that both constants,  $k_{LC}$  and  $k_{IHB}$ , decrease monotonically as  $d$  increases. When  $d$  is large, both rate constants  $k_{IHB}$  and  $k_{LC}$  also no longer change with  $d$ . It also shows that the HB breaking rate constant  $k_{IHB}$  is relatively larger than  $k_{LC}$ . This difference is related to the definitions of HB populations,  $h(t)$  and  $h^{(s)}(t)$ . The definition of  $h^{(s)}(t)$  leads to an increased HB break rate at the interface. The LC method retains the original rate constant of H-bonds but may include contributions from bulk water molecules.

Similar to the HB autocorrelation functions, we have the equations  $dk/dd = 0$ , for  $k_{IHB}$  and  $k_{LC}$ , with respect to  $d$ . For  $K = k_{IHB}$  and  $K = k_{LC}$ , we identify solutions  $d_{f1}'$  and  $d_{f2}'$ , respectively. Here  $d_{f1}'$  and  $d_{f2}'$  represent the HB reaction rate-based thickness of the interface obtained from the LC and IHB

method, respectively. We then calculate the thickness of the real air–water interface as  $d_f' = (d_{f1}' + d_{f2}')/2 \approx 4 \text{ \AA}$ . This result is supported by our calculation of the  $d$ -dependence of the HB reforming rate constants, namely,  $k_{LC}'$  and  $k_{IH\beta}'$ . For more details, please refer to Figure S9 in Supporting Information.

**3.3. Orientational Relaxation of the OH Stretch and Other Supports.** To verify our conclusion on the thickness of the air–water interface from the interfacial HB dynamics, we performed calculations on the orientational relaxation of the OH stretch from the perspective of anisotropy decay.<sup>96</sup>

As shown in Figure 5a, the orientation correlation function fits well with a biexponential decay function. The two

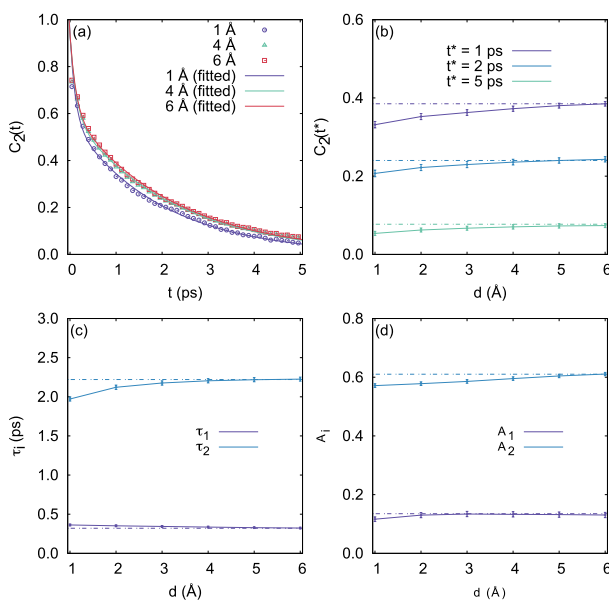


**Figure 5.** Orientation correlation function  $C_2(t)$  for the air–water interface. (a)  $C_2(t)$  for  $d = 1, 4, 6 \text{ \AA}$  and the biexponential decay function  $C_2(t) = A_1 \exp(t/\tau_1) + A_2 \exp(t/\tau_2)$ .  $d$ -dependence of (b)  $C_2(t^*)$  for water molecules at the air–water interface with  $t^* = 1, 2, 5 \text{ (ps)}$ ; (c) relaxation time ( $\tau_1$  and  $\tau_2$ ), and (d) the amplitude ( $A_1$  and  $A_2$ ). Dotted line is a horizontal line for easier viewing. As  $d$  increases to  $d = 4 \text{ \AA}$ ,  $C_2(t^*)$  and  $\tau_\nu$ ,  $A_i$  all converge to a fixed value, respectively. (We also obtained consistent results for systems with 125 and 216 water molecules, please refer to Supporting Information.).

relaxation rates ( $1/\tau_1$  and  $1/\tau_2$ ) differ; the larger relaxation time  $\tau_2$  increases with the increase of  $d$ , while the smaller one,  $\tau_1$ , remains relatively unchanged with variations in  $d$ . In Figure 5b, the values of the orientational correlation function  $C_2(t) = \langle P_2(\hat{u}(0)\hat{u}(t)) \rangle$  at three reference time  $t^* = 1, 2, 5 \text{ (ps)}$  are plotted. At all these times,  $C(t^*)$  increases with increasing  $d$  and no longer increases significantly for  $d \geq 4 \text{ \AA}$ .

Similar to the earlier results on HB population correlation functions and the HB reaction rates, as  $d$  increases,  $C_2(t^*)$  and associated relaxation times converge to a fixed value, respectively, which characterizes the decay time of the orientation relaxation process of OH bonds. From the convergence trend of the relaxation times and corresponding amplitudes in Figure 5c,d, we find that at the interface with a thickness greater than  $4 \text{ \AA}$ , the OH orientation relaxation of the air–water interface is no longer different from bulk water.

Experimentally, the information on the interface molecules can be obtained from the SFG spectrum. The vibration relaxation time of the interface water molecules can be obtained based on the SFG spectrum using analysis techniques such as Singular Value Decomposition (SVD).<sup>97</sup> We also defined the interface molecule orientation relaxation time from the  $C_2(t)$  correlation of the interface water molecules. However, due to the arbitrariness of the specific form of defining the relaxation time, the results we obtained cannot be directly and accurately compared with the experimental results. Because of the current huge challenges in directly measuring water, we compared the data obtained from interfacial HB dynamics, interfacial OH orientation relaxation dynamics, and AIMD simulations. Our results from interfacial HB dynamics are consistent with the results from  $C_2(t)$  and density profile from AIMD simulations of the air–water interface. Furthermore, the interface thickness aligns with values obtained through experimental measurements and AIMD simulations, as detailed in Table 1. Therefore, we arrive at a consistent

**Table 1.** Air–Water Interface Thickness Obtained by Experiments and Computer Simulations

methods	$T \text{ (K)}$	$d \text{ (\AA)}$
ellipsometry (Rayleigh)	293.15	3.0
ellipsometry (Raman and Ramdas <sup>27</sup> )	293	5.0
ellipsometry (McBain et al. <sup>28</sup> )	293	$\geq 2.26$
ellipsometry (Kinoshita and Yokota <sup>29</sup> )	293	7.1
X-ray reflectivity (Braslau et al. <sup>32</sup> )	298	$3.24 \pm 0.05$
DeePMD/MB-pol/Free OH (this work)	300	5.0
BOMD/BLYP-D3/LC&IH $\beta$ (this work)	300	4.0
DeePMD/MB-pol/LC&IH $\beta$ (this work)	300	4.0

conclusion on the issue of estimating the thickness of the air–water interface, from the perspective of HB dynamics and OH reorientation relaxation.

There is one more aspect worth noting when studying the air–water interface based on the aforementioned definition of H-bonds. Some complications arise in interpreting vibrational SFG spectroscopy results.<sup>98</sup> An alternative perspective focusing on nonbonded OH groups better establishes a direct correlation between free OH and the  $3700 \text{ cm}^{-1}$  peak, typically attributed to free OH groups.<sup>98</sup> Considering the dynamics of free OH groups, the thickness of the air–water interface is also estimated from simulations. Details on the methods and results can be found in Supporting Information. From the  $d$ -dependence of the interfacial free OH correlation function, we determined an interface thickness of approximately  $5 \text{ \AA}$ . As shown in Table 1, this value slightly deviates from the main results presented in this paper, highlighting that the measured thickness of the air–water interface varies depending on the properties of interest. Thus, to accurately determine the water interface thickness, it is essential to integrate findings from these varied perspectives.

#### 4. CONCLUSIONS

In this study, we have developed a two-extreme approach to investigate the HB dynamics at the air–water interface and to determine the interface's thickness. One extreme scenario underestimates the HB breaking rate constant, while the other overestimates it, implying that each scenario provides only a partial insight into the interfacial HB dynamics. Subsequently, based on DFTMD and DeePMD simulations, we have applied

our approach to two distinct system properties: HB relaxation and HB reaction rate constants at the air–water interface. Our results across both properties indicate that the predictions from both extreme scenarios converge as the thickness of the air–water interface increases to 4 Å. Thus, we have reason to believe the thickness, which falls between these two extremes, converges at this critical value.

This work introduces an approach to complement existing ones for investigating the air–water interface from a fresh perspective. Through HB dynamics of the air–water interface, interfacial properties, such as thickness in this case, can be obtained through a method analogous to the squeeze theorem. Beyond the scope of HB dynamics, this approach can be extended to other properties like molecular orientation distribution,<sup>99,100</sup> free OH dynamics,<sup>98</sup> and SFG spectrum,<sup>11,13,41</sup> or other systems like solution interfacial surfaces where statistical properties of the interface and bulk phase differ significantly. Looking ahead, this study could inspire further research into ions' hydration shells by examining ions' effects through HB dynamics.

It is important to note that our current approach focuses on probing the local environment by analyzing water pairs within HB dynamics, without considering the collective behaviors of water molecules in the HB networks. However, the collective dynamics of many water molecules have been increasingly discussed in recent research, demonstrating a close relationship with observable properties such as dielectric spectroscopy and time-dependent vibrational spectroscopy.<sup>101–106</sup> We hope our study will inspire further innovative ideas on related topics by incorporating considerations of the collective nature of water.

## ASSOCIATED CONTENT

### Data Availability Statement

The codes utilized in this study are publicly accessible on GitHub at [https://github.com/hg08/hb\\_ihb](https://github.com/hg08/hb_ihb).

### Supporting Information

The Supporting Information is available free of charge at <https://pubs.acs.org/doi/10.1021/acs.jctc.4c00457>.

Hydrogen bond correlation functions, HB breaking and reforming rate constants, details of Scenario 1: the LC method, rotational anisotropy decay of OH stretch at the air–water interface, computational methods including DFTMD and DeePMD simulations, results based on DFTMD simulations for systems in other sizes, results based on DeePMD simulations for systems in other sizes, and perspectives derived from the correlation function of free OH groups ([PDF](#))

## AUTHOR INFORMATION

### Corresponding Author

Jie Huang – Department of Applied Physics, Aalto University, Helsinki FI-00076, Finland;  [orcid.org/0000-0003-3560-283X](https://orcid.org/0000-0003-3560-283X); Email: [jie.huang@aalto.fi](mailto:jie.huang@aalto.fi)

### Author

Gang Huang – Institute of Theoretical Physics, Chinese Academy of Sciences, 100190 Beijing, China;  [orcid.org/0000-0001-8515-8584](https://orcid.org/0000-0001-8515-8584)

Complete contact information is available at:  
<https://pubs.acs.org/10.1021/acs.jctc.4c00457>

## Notes

The authors declare no competing financial interest.

## ACKNOWLEDGMENTS

This work was supported by the CSC—Chinese Government Scholarship (No. 2011113214). G.H. thanks Yuliang Jin, Rémi Khatib and Marialore Sulpizi for insightful discussions. The DFTMD simulations were conducted on the Magon ZDV cluster in Mainz and the Cray XE6 (Hermit) at the HRLS supercomputing center in Stuttgart. The DeePMD simulations were performed on Triton, provided by Aalto Science-IT project.

## REFERENCES

- (1) Morita, A.; Hynes, J. T. A Theoretical Analysis of the Sum Frequency Generation Spectrum of the Water Surface. *J. Chem. Phys.* **2000**, *123*, 371–390.
- (2) Jungwirth, P.; Tobias, D. J. Molecular Structure of Salt Solutions: A New View of the Interface with Implications for Heterogeneous Atmospheric Chemistry. *J. Phys. Chem. B* **2001**, *105*, 10468–10472.
- (3) Wilson, K. R.; Schaller, R. D.; Co, D. T.; Saykally, R. J.; Rude, B. S.; Catalano, T.; Bozek, J. D. Surface Relaxation in Liquid Water and Methanol Studied by X-Ray Absorption Spectroscopy. *J. Chem. Phys.* **2002**, *117*, 7738–7744.
- (4) Raymond, E. A.; Tarbuck, T. L.; Brown, M. G.; Richmond, G. L. Hydrogen-Bonding Interactions at the Vapor/Water Interface Investigated by Vibrational Sum-Frequency Spectroscopy of HOD/H<sub>2</sub>O/D<sub>2</sub>O Mixtures and Molecular Dynamics Simulations. *J. Phys. Chem. B* **2003**, *107*, 546–556.
- (5) Shen, Y. R.; Ostroverkhov, V. Sum-Frequency Vibrational Spectroscopy on Water Interfaces: Polar Orientation of Water Molecules at Interfaces. *Chem. Rev.* **2006**, *106*, 1140–1154.
- (6) Smits, M.; Ghosh, A.; Sterrer, M.; Müller, M.; Bonn, M. Ultrafast Vibrational Energy Transfer between Surface and Bulk Water at the Air-Water Interface. *Phys. Rev. Lett.* **2007**, *98*, No. 098302.
- (7) Sovago, M.; Campen, R. K.; Wurpel, G. W. H.; Müller, M.; Bakker, H. J.; Bonn, M. Vibrational Response of Hydrogen-Bonded Interfacial Water is Dominated by Intramolecular Coupling. *Phys. Rev. Lett.* **2008**, *100*, No. 173901.
- (8) Sovago, M.; Kramer Campen, R.; Bakker, H. J.; Bonn, M. Hydrogen Bonding Strength of Interfacial Water Determined with Surface Sum-Frequency Generation. *Chem. Phys. Lett.* **2009**, *470*, 7–12.
- (9) Stiopkin, I. V.; Weeraman, C.; Pieniazek, P. A.; Shalhout, F. Y.; Skinner, J. L.; Benderskii, A. V. Hydrogen Bonding at the Water Surface Revealed by Isotopic Dilution Spectroscopy. *Nature* **2011**, *474*, 192.
- (10) Hsieh, C.-S.; Campen, R. K.; Vila Verde, A. C.; Bolhuis, P.; Nienhuys, H.-K.; Bonn, M. Ultrafast Reorientation of Dangling OH Groups at the Air-Water Interface Using Femtosecond Vibrational Spectroscopy. *Phys. Rev. Lett.* **2011**, *107*, No. 116102.
- (11) Nihonyanagi, S.; Ishiyama, T.; Lee, T.-K.; Yamaguchi, S.; Bonn, M.; Morita, A.; Tahara, T. Unified Molecular View of the Air/Water Interface Based on Experimental and Theoretical  $\chi^{(2)}$  Spectra of an Isotopically Diluted Water Surface. *J. Am. Chem. Soc.* **2011**, *133*, 16875–16880.
- (12) Singh, P. C.; Nihonyanagi, S.; Yamaguchi, S.; Tahara, T. Interfacial Water in the Vicinity of a Positively Charged Interface Studied by Steady-State and Time-Resolved Heterodyne-Detected Vibrational Sum Frequency Generation. *J. Chem. Phys.* **2014**, *141*, 18C527.
- (13) Nihonyanagi, S.; Kusaka, R.; Inoue, K.-i.; Adhikari, A.; Yamaguchi, S.; Tahara, T. Accurate Determination of Complex  $\chi^{(2)}$  Spectrum of the Air/Water Interface. *J. Chem. Phys.* **2015**, *143*, 124707.
- (14) Ishiyama, T. Energy Relaxation Path of Excited Free OH Vibration at an Air/Water Interface Revealed by Nonequilibrium Ab

- Initio Molecular Dynamics Simulation. *J. Chem. Phys.* **2021**, *154*, 104708.
- (15) Ahmed, M.; Nihonyanagi, S.; Tahara, T. Ultrafast Vibrational Dynamics of the Free OD at the Air/Water Interface: Negligible Isotopic Dilution Effect but Large Isotope Substitution Effect. *J. Chem. Phys.* **2022**, *156*, 224701.
- (16) Omranpour, A.; Hijes, D.; Montero, P.; Behler, J.; Dellago, C. Perspective: Atomistic Simulations of Water and Aqueous Systems with Machine Learning Potentials. *arXiv* **2024**. preprint arXiv:2401.17875.
- (17) Lee, C.; McCammon, J. A.; Rossky, P. J. The Structure of Liquid Water at an Extended Hydrophobic Surface. *J. Chem. Phys.* **1984**, *80*, 4448–4455.
- (18) Dang, L. X.; Chang, T.-M. Molecular Dynamics Study of Water Clusters, Liquid, and Liquid-Vapour Interface of Water with Many-Body Potentials. *J. Chem. Phys.* **1997**, *106*, 8149.
- (19) Hsieh, C.-S.; Campen, R. K.; Okuno, M.; Backus, E. H. G.; Nagata, Y.; Bonn, M. Mechanism of Vibrational Energy Dissipation of Free OH Groups at the Air-Water Interface. *Proc. Natl. Acad. Sci. U.S.A.* **2013**, *110*, 18780–18785.
- (20) Liu, P.; Harder, E.; Berne, B. J. Hydrogen-Bond Dynamics in the Air-Water Interface. *J. Phys. Chem. B* **2005**, *109*, 2949–2955.
- (21) Gan, W.; Wu, D.; Zhang, Z.; Feng, R.-r.; Wang, H.-f. Polarization and Experimental Configuration Analyses of Sum Frequency Generation Vibrational Spectra, Structure, and Orientational Motion of the Air/Water Interface. *J. Chem. Phys.* **2006**, *124*, 114705.
- (22) McGuire, J. A.; Shen, Y. R. Ultrafast Vibrational Dynamics at Water Interfaces. *Science* **2006**, *313*, 1945–1948.
- (23) Singh, P. C.; Nihonyanagi, S.; Yamaguchi, S.; Tahara, T. Communication: Ultrafast Vibrational Dynamics of Hydrogen Bond Network Terminated at the Air/Water Interface: A Two-Dimensional Heterodyne-Detected Vibrational Sum Frequency Generation Study. *J. Chem. Phys.* **2013**, *139*, 161101.
- (24) Inoue, K.-i.; Ishiyama, T.; Nihonyanagi, S.; Yamaguchi, S.; Morita, A.; Tahara, T. Efficient Spectral Diffusion at the Air/Water Interface Revealed by Femtosecond Time-Resolved Heterodyne-Detected Vibrational Sum Frequency Generation Spectroscopy. *J. Phys. Chem. Lett.* **2016**, *7*, 1811–1815.
- (25) Jeon, J.; Hsieh, C.-S.; Nagata, Y.; Bonn, M.; Cho, M. Hydrogen Bonding and Vibrational Energy Relaxation of Interfacial Water: A Full DFT Molecular Dynamics Simulation. *J. Chem. Phys.* **2017**, *147*, No. 044707.
- (26) Ojha, D.; Kühne, T. Hydrogen Bond Dynamics of Interfacial Water Molecules Revealed from Two-Dimensional Vibrational Sum-Frequency Generation Spectroscopy. *Sci. Rep.* **2021**, *11*, 2456.
- (27) Raman, C.; Ramdas, L. On the Thickness of the Optical Transition Layer in Liquid Surfaces. *Philos. Mag.* **1927**, *3*, 220.
- (28) McBain, J. W.; Bacon, R. C.; Bruce, H. D. Optical Surface Thickness of Pure Water. *J. Chem. Phys.* **1939**, *7*, 818–823.
- (29) Kinoshita, K.; Yokota, H. Temperature Dependence of the Optical Surface Thickness of Water. *J. Phys. Soc. Jpn.* **1965**, *20*, 1086.
- (30) Fumagalli, L.; Esfandiar, A.; Fabregas, R.; Hu, S.; Ares, P.; Janardanan, A.; Yang, Q.; B, R.; Taniguchi, T.; Watanabe, K.; Gomila, G.; Novoselov, K. S.; Geim, A. K. Anomalously Low Dielectric Constant of Confined Water. *Science* **2018**, *360*, 1339–1342.
- (31) Braslav, A.; Deutsch, M.; Pershan, P. S.; Weiss, A. H.; Als-Nielsen, J.; Bohr, J. Surface Roughness of Water Measured by X-Ray Reflectivity. *Phys. Rev. Lett.* **1985**, *54*, 114–117.
- (32) Braslav, A.; Pershan, P. S.; Swislow, G.; Ocko, B. M.; Als-Nielsen, J. Capillary Waves on the Surface of Simple Liquids Measured by X-Ray Reflectivity. *Phys. Rev. A* **1988**, *38*, 2457–2470.
- (33) Superfine, R.; Huang, J. H.; Shen, Y. R. Nonlinear Optical Studies of the Pure Liquid/Vapor Interface: Vibrational Spectra and Polar Ordering. *Phys. Rev. Lett.* **1991**, *66*, 1066–1069.
- (34) Du, Q.; Superfine, R.; Freysz, E.; Shen, Y. R. Vibrational Spectroscopy of Water at the Vapor/Water Interface. *Phys. Rev. Lett.* **1993**, *70*, 2313–2316.
- (35) Ostroverkhov, V.; Waychunas, G. A.; Shen, Y. R. New Information on Water Interfacial Structure Revealed by Phase-Sensitive Surface Spectroscopy. *Phys. Rev. Lett.* **2005**, *94*, No. 046102.
- (36) Groenzin, H.; Li, I.; Buch, V.; Shultz, M. J. The Single-Crystal, Basal Face of Ice Ih Investigated with Sum Frequency Generation. *J. Chem. Phys.* **2007**, *127*, 214502.
- (37) Shen, Y. R. Basic Theory of Surface Sum-Frequency Generation. *J. Phys. Chem. C* **2012**, *116*, 15505–15509.
- (38) Ishiyama, T.; Takahashi, H.; Morita, A. Origin of Vibrational Spectroscopic Response at Ice Surface. *J. Phys. Chem. Lett.* **2012**, *3*, 3001.
- (39) Shen, Y. R. Phase-Sensitive Sum-Frequency Spectroscopy. *Annu. Rev. Phys. Chem.* **2013**, *64*, 129–150.
- (40) Ohto, T.; Usui, K.; Hasegawa, T.; Bonn, M.; Nagata, Y. Toward Ab Initio Molecular Dynamics Modeling for Sum-Frequency Generation Spectra; an Efficient Algorithm based on Surface-Specific Velocity-Velocity Correlation Function. *J. Chem. Phys.* **2015**, *143*, 124702.
- (41) Tang, F.; Ohto, T.; Sun, S.; Rouxel, J. R.; Imoto, S.; Backus, E. H. G.; Mukamel, S.; Bonn, M.; Nagata, Y. Molecular Structure and Modeling of Water-Air and Ice-Air Interfaces Monitored by Sum-Frequency Generation. *Chem. Rev.* **2020**, *120*, 3633–3667.
- (42) Kuo, I.-F. W.; Mundy, C. J.; Eggemann, B. L.; McGrath, M. J.; Siepmann, J. I.; Chen, B.; Vieceli, J.; Tobias, D. J. Structure and Dynamics of the Aqueous Liquid-Vapor Interface: A Comprehensive Particle-Based Simulation Study. *J. Phys. Chem. B* **2006**, *110*, 3738–3746.
- (43) Wick, C. D.; Kuo, I.-F. W.; Mundy, C. J.; Dang, L. X. The Effect of Polarizability for Understanding the Molecular Structure of Aqueous Interfaces. *J. Chem. Theory Comput.* **2007**, *3*, 2002–2010.
- (44) Morita, A.; Garrett, B. C. Molecular Theory of Mass Transfer Kinetics and Dynamics at Gas-Water Interface. *Fluid Dyn. Res.* **2008**, *40*, 459.
- (45) Sedlmeier, F.; Horinek, D.; Netz, R. R. Nanoroughness, Intrinsic Density Profile, and Rigidity of the Air-Water Interface. *Phys. Rev. Lett.* **2009**, *103*, No. 136102.
- (46) Fan, Y.; Chen, X.; Yang, L.; Cremer, P. S.; Gao, Y. Q. On the Structure of Water at the Aqueous/Air Interface. *J. Phys. Chem. B* **2009**, *113*, 11672–11679.
- (47) Ishiyama, T.; Morita, A. Analysis of Anisotropic Local Field in Sum Frequency Generation Spectroscopy with the Charge Response Kernel Water Model. *J. Chem. Phys.* **2009**, *131*, 244714.
- (48) Willard, A. P.; Chandler, D. Instantaneous Liquid Interfaces. *J. Phys. Chem. B* **2010**, *114*, 1954.
- (49) Vila Verde, A.; Bolhuis, P. G.; Campen, R. K. Statics and Dynamics of Free and Hydrogen-Bonded OH Groups at the Air/Water Interface. *J. Phys. Chem. B* **2012**, *16*, 9467–9481.
- (50) Ishiyama, T.; Morita, A.; Tahara, T. Molecular Dynamics Study of Two-Dimensional Sum Frequency Generation Spectra at Vapor/Water Interface. *J. Chem. Phys.* **2015**, *142*, 212407.
- (51) Nagata, Y.; Hasegawa, T.; Backus, E. H. G.; Usui, K.; Yoshimune, S.; Ohto, T.; Bonn, M. The Surface Roughness, but not the Water Molecular Orientation Varies with Temperature at the Water-Air Interface. *Phys. Chem. Chem. Phys.* **2015**, *17*, 23559.
- (52) Kühne, T. D.; Pascal, T. A.; Kaxiras, E.; Jung, Y. New Insights into the Structure of the Vapor/Water Interface from Large-Scale First-Principles Simulations. *J. Phys. Chem. Lett.* **2011**, *2*, 105–113.
- (53) Nagata, Y.; Pool, R. E.; Backus, E. H. G.; Bonn, M. Nuclear Quantum Effects Affect Bond Orientation of Water at the Water-Vapor Interface. *Phys. Rev. Lett.* **2012**, *109*, No. 226101.
- (54) Kessler, J.; Elgarbary, H.; Spura, T.; Karhan, K.; Partovi-Azar, P.; Hassanali, A. A.; Kühne, T. D. Structure and Dynamics of the Instantaneous Water/Vapor Interface Revisited by Path-Integral and Ab Initio Molecular Dynamics Simulations. *J. Phys. Chem. B* **2015**, *119*, 10079–10086.
- (55) Ohto, T.; Dodia, M.; Xu, J.; Imoto, S.; Tang, F.; Zysk, F.; Kühne, T. D.; Shigeta, Y.; Bonn, M.; Nagata, Y. Assessing the Accuracy of Density Functional Theory through Structure and

- Dynamics of the Water-Air Interface. *J. Phys. Chem. Lett.* **2019**, *10*, 4914–4919.
- (56) Jungwirth, P.; Tobias, D. J. Specific Ion Effects at the Air/Water Interface. *Chem. Rev.* **2006**, *106*, 1259–1281.
- (57) Baer, M. D.; Kuo, I.-F. W.; Tobias, D. J.; Mundy, C. J. Toward a Unified Picture of the Water Self-Ions at the Air-Water Interface: A Density Functional Theory Perspective. *J. Phys. Chem. B* **2014**, *118*, 8364–8372.
- (58) Nguyen, C. V.; Nakahara, H.; Phan, C. M. Surface Potential of the Air/Water Interface. *J. Oleo Sci.* **2020**, *69*, 519–528.
- (59) Peng, Y.; Tong, Z.; Yang, Y.; Sun, C. Q. The Common and Intrinsic Skin Electric-Double-Layer (EDL) and Its Bonding Characteristics of Nanostructures. *Appl. Surf. Sci.* **2021**, *539*, No. 148208.
- (60) Townsend, R. M.; Gryko, J.; Rice, S. A. Structure of the Liquid-Vapor Interface of Water. *J. Chem. Phys.* **1985**, *82*, 4391–4392.
- (61) Wilson, M. A.; Pohorille, A.; Pratt, L. R. Molecular Dynamics of the Water Liquid-Vapor Interface. *J. Phys. Chem.* **1987**, *91*, 4873–4878.
- (62) Matsumoto, M.; Kataoka, Y. Study on Liquid-Vapor Interface of Water. I. Simulational Results of Thermodynamic Properties and Orientational Structure. *J. Chem. Phys.* **1988**, *88*, 3233–3245.
- (63) Townsend, R. M.; Rice, S. A. Molecular Dynamics Studies of the Liquid-Vapor Interface of Water. *J. Chem. Phys.* **1991**, *94*, 2207–2218.
- (64) Lie, G. C.; Grigoras, S.; Dang, L. X.; Yang, D.; McLean, A. D. Monte Carlo Simulation of the Liquid-Vapor Interface of Water Using an Ab Initio Potential. *J. Chem. Phys.* **1993**, *99*, 3933–3937.
- (65) Alejandre, J.; Tildesley, D. J.; Chapela, G. A. Molecular Dynamics Simulation of the Orthobaric Densities and Surface Tension of Water. *J. Chem. Phys.* **1995**, *102*, 4574–4583.
- (66) Taylor, R. S.; Dang, L. X.; Garrett, B. C. Molecular Dynamics Simulations of the Liquid/Vapor Interface of SPC/E Water. *J. Phys. Chem.* **1996**, *100*, 11720–11725.
- (67) Dang, L. X.; Chang, T.-M. Molecular Dynamics Study of Water Clusters, Liquid, and Liquid-Vapor Interface of Water with Many-Body Potentials. *J. Chem. Phys.* **1997**, *106*, 8149–8159.
- (68) Car, R.; Parrinello, M. Unified Approach for Molecular Dynamics and Density Functional Theory. *Phys. Rev. Lett.* **1985**, *55*, 2471–2474.
- (69) Marx, D.; Hutter, J. Ab Initio Molecular Dynamics: Theory and Implementation. In *Modern Methods and Algorithms of Quantum Chemistry*, Grotendorst, J., Ed.; NIC Series; John von Neumann Institute for Computing: Jülich, 2000; Vol. 1, pp 301–499.
- (70) Car, R. Introduction to Density-Functional Theory and Ab-Initio Molecular Dynamics. *Quant. Struct. Act. Rel.* **2002**, *21*, 97–104.
- (71) Kuo, I.-F. W.; Mundy, C. J. An Ab Initio Molecular Dynamics Study of the Aqueous Liquid-Vapor Interface. *Science* **2004**, *303*, 658–660.
- (72) Kühne, T. D.; Krack, M.; Mohamed, F. R.; Parrinello, M. Efficient and Accurate Car-Parrinello-like Approach to Born-Oppenheimer Molecular Dynamics. *Phys. Rev. Lett.* **2007**, *98*, No. 066401.
- (73) Khaliullin, R. Z.; Kühne, T. D. Microscopic Properties of Liquid Water from Combined Ab Initio Molecular Dynamics and Energy Decomposition Studies. *Phys. Chem. Chem. Phys.* **2013**, *15*, 15746–15766.
- (74) Blas, F. J.; Rio, E. M. D.; Miguel, E. D.; Jackson, G. An Examination of the Vapour-Liquid Interface of Associating Fluids Using a SAFT-DFT Approach. *Mol. Phys.* **2001**, *99*, 1851–1865.
- (75) Pezzotti, S.; Galimberti, D. R.; Gaigeot, M.-P. 2D H-Bond Network as the Topmost Skin to the Air-Water Interface. *J. Phys. Chem. Lett.* **2017**, *8*, 3133–3141.
- (76) Schran, C.; Thiemann, F. L.; Rowe, P.; Müller, E. A.; Marsalek, O.; Michaelides, A. Machine Learning Potentials for Complex Aqueous Systems Made Simple. *Proc. Natl. Acad. Sci. U. S. A.* **2021**, *118*, No. e2110077118.
- (77) Zeng, J.; Zhang, D.; Lu, D.; Mo, P.; Li, Z.; Chen, Y.; Rynik, M.; Huang, L.; Li, Z.; Shi, S.; Wang, Y.; Ye, H.; Tu, P.; Yang, J.; Ding, Y.; Li, Y.; Tisi, D.; Zeng, Q.; Bao, H.; Xia, Y.; Huang, J.; Muraoka, K.; Wang, Y.; Chang, J.; Yuan, F.; Bore, S. L.; Cai, C.; Lin, Y.; Wang, B.; Xu, J.; Zhu, J.-X.; Luo, C.; Zhang, Y.; Goodall, R. E. A.; Liang, W.; Singh, A. K.; Yao, S.; Zhang, J.; Wentzcovitch, R.; Han, J.; Liu, J.; Jia, W.; York, D. M.; E, W.; Car, R.; Zhang, L.; Wang, H. DeePMD-kit v2: A Software Package for Deep Potential Models. *J. Chem. Phys.* **2023**, *159*, No. 054801.
- (78) Babin, V.; Leforestier, C.; Paesani, F. Development of a "First Principles" Water Potential with Flexible Monomers: Dimer Potential Energy Surface, VRT Spectrum, and Second Virial Coefficient. *J. Chem. Theory Comput.* **2013**, *9*, 5395–5403.
- (79) Babin, V.; Medders, G. R.; Paesani, F. Development of a "First Principles" Water Potential with Flexible Monomers. II: Trimer Potential Energy Surface, Third Virial Coefficient, and Small Clusters. *J. Chem. Theory Comput.* **2014**, *10*, 1599–1607.
- (80) Medders, G. R.; Babin, V.; Paesani, F. Development of a "First-Principles" Water Potential with Flexible Monomers. III. Liquid Phase Properties. *J. Chem. Theory Comput.* **2014**, *10*, 2906–2910.
- (81) Bore, S. L.; Paesani, F. Realistic Phase Diagram of Water from "First Principles" Data-Driven Quantum Simulations. *Nat. Commun.* **2023**, *14*, 3349.
- (82) Muniz, M. C.; Gartner, I.; Thomas, E.; Riera, M.; Knight, C.; Yue, S.; Paesani, F.; Panagiotopoulos, A. Z. Vapor–Liquid Equilibrium of Water with the MB-pol Many-Body Potential. *J. Chem. Phys.* **2021**, *154*, 211103.
- (83) Medders, G. R.; Paesani, F. Dissecting the Molecular Structure of the Air/Water Interface from Quantum Simulations of the Sum-Frequency Generation Spectrum. *J. Am. Chem. Soc.* **2016**, *138*, 3912–3919.
- (84) Luzar, A.; Chandler, D. Hydrogen-Bond Kinetics in Liquid Water. *Nature* **1996**, *379*, 55–57.
- (85) Giberti, F.; Hassanali, A. A. The Excess Proton at the Air-Water Interface: The Role of Instantaneous Liquid Interfaces. *J. Chem. Phys.* **2017**, *146*, 244703.
- (86) Beaglehole, D.; Wilson, P. Thickness and Anisotropy of the Ice-Water Interface. *J. Phys. Chem.* **1993**, *97*, 11053–11055.
- (87) Sokhan, V. P.; Tildesley, D. J. The Free Surface of Water: Molecular Orientation, Surface Potential and Nonlinear Susceptibility. *Mol. Phys.* **1997**, *92*, 625–640.
- (88) Paul, S.; Chandra, A. Hydrogen Bond Dynamics at Vapour-Water and Metal-Water Interfaces. *Chem. Phys. Lett.* **2004**, *386*, 218–224.
- (89) Morita, A. Improved Computation of Sum Frequency Generation Spectrum of the Surface of Water. *J. Phys. Chem. B* **2006**, *110*, 3158–3163.
- (90) Zhao, J.; Yao, G.; Ramisetti, S. B.; Hammond, R. B.; Wen, D. Molecular Dynamics Simulation of the Salinity Effect on the n-Decane/Water/Vapor Interfacial Equilibrium. *Energy Fuels* **2018**, *32*, 11080–11092.
- (91) Serva, A.; Pezzotti, S.; Bougueroua, S.; Galimberti, D. R.; Gaigeot, M.-P. Combining Ab-Initio and Classical Molecular Dynamics Simulations to Unravel the Structure of the 2D-HB-Network at the Air-Water Interface. *J. Mol. Struct.* **2018**, *1165*, 71–78.
- (92) Madarász, A.; Rossky, P. J.; Turi, L. Excess Electron Relaxation Dynamics at Water/Air Interfaces. *J. Chem. Phys.* **2007**, *126*, 234707.
- (93) Luzar, A. Resolving the Hydrogen Bond Dynamics Conundrum. *J. Chem. Phys.* **2000**, *113*, 10663.
- (94) Benjamin, I. Hydrogen Bond Dynamics at Water/Organic Liquid Interfaces. *J. Phys. Chem. B* **2005**, *109*, 13711–13715.
- (95) Luzar, A.; Chandler, D. Structure and Hydrogen Bond Dynamics of Water–Dimethyl Sulfoxide Mixtures by Computer Simulations. *J. Chem. Phys.* **1993**, *98*, 8160–8173.
- (96) Moilanen, D. E.; Fenn, E. E.; Lin, Y.-S.; Skinner, J. L.; Bagchi, B.; Fayer, M. D. Water Inertial Reorientation: Hydrogen Bond Strength and the Angular Potential. *Proc. Natl. Acad. Sci. U.S.A.* **2008**, *105*, 5295–5300.
- (97) ichi Inoue, K.; Ahmed, M.; Nihonyanagi, S.; Tahara, T. Reorientation-Induced Relaxation of Free OH at the Air/Water

- Interface Revealed by Ultrafast Heterodyne-Detected Nonlinear Spectroscopy. *Nat. Commun.* **2020**, *11*, 5344.
- (98) Tang, F.; Ohto, T.; Hasegawa, T.; Xie, W. J.; Xu, L.; Bonn, M.; Nagata, Y. Definition of Free O–H Groups of Water at the Air–Water Interface. *J. Chem. Theory Comput.* **2018**, *14*, 357–364.
- (99) Rao, Y.; Tao, Y.-s.; Wang, H.-f. Quantitative Analysis of Orientational Order in the Molecular Monolayer by Surface Second Harmonic Generation. *J. Chem. Phys.* **2003**, *119*, 5226–5236.
- (100) Gan, W.; Wu, D.; Zhang, Z.; Feng, R.-r.; Wang, H.-f. Polarization and Experimental Configuration Analyses of Sum Frequency Generation Vibrational Spectra, Structure, and Orientational Motion of the Air/Water Interface. *J. Chem. Phys.* **2006**, *124*, 114705.
- (101) Popov, I.; Ishai, P. B.; Khamzin, A.; Feldman, Y. The Mechanism of the Dielectric Relaxation in Water. *Phys. Chem. Chem. Phys.* **2016**, *18*, 13941–13953.
- (102) Fecko, C. J.; Eaves, J. D.; Loparo, J. J.; Tokmakoff, A.; Geissler, P. L. Ultrafast Hydrogen-Bond Dynamics in the Infrared Spectroscopy of Water. *Science* **2003**, *301*, 1698–1702.
- (103) Fecko, C. J.; Loparo, J. J.; Roberts, S. T.; Tokmakoff, A. Local Hydrogen Bonding Dynamics and Collective Reorganization in Water: Ultrafast Infrared Spectroscopy of HOD/D<sub>2</sub>O. *J. Chem. Phys.* **2005**, *122*, No. 054506.
- (104) Hörlz, C.; Forbert, H.; Marx, D. Dielectric Relaxation of Water: Assessing the Impact of Localized Modes, Translational Diffusion, and Collective Dynamics. *Phys. Chem. Chem. Phys.* **2021**, *23*, 20875–20882.
- (105) Offei-Danso, A.; Morzan, U. N.; Rodriguez, A.; Hassanali, A.; Jelic, A. The Collective Burst Mechanism of Angular Jumps in Liquid Water. *Nat. Commun.* **2023**, *14*, 1345.
- (106) Malosso, C.; Manko, N.; Izzo, M. G.; Baroni, S.; Hassanali, A. Evidence of Ferroelectric Features in Low-Density Supercooled Water from Ab Initio Deep Neural-Network Simulations. *Proc. Natl. Acad. Sci. U. S. A.* **2024**, *121*, No. e2407295121.



CAS BIOFINDER DISCOVERY PLATFORM™  
**PRECISION DATA  
FOR FASTER  
DRUG  
DISCOVERY**

CAS BioFinder helps you identify  
targets, biomarkers, and pathways

Unlock insights

**CAS**  
A division of the  
American Chemical Society

# **Supporting Information for**

## **Revisiting the Thickness of the Air-Water Interface from Two Extremes of Interface Hydrogen Bond Dynamics**

Gang Huang<sup>†</sup> and Jie Huang<sup>\*,‡</sup>

<sup>†</sup> *Institute of Theoretical Physics, Chinese Academy of Sciences, Zhongguancun East Road 55, 100190 Beijing, China*

<sup>‡</sup> *Department of Applied Physics, Aalto University, Helsinki FI-00076, Finland*

E-mail: jie.huang@aalto.fi

## **1 Hydrogen bond correlation functions**

Using a geometric criterion of HB, Luzar and Chandler<sup>1</sup> have pioneered the analysis of HB dynamics of pure water, and subsequently, such analysis has been extended to more complex systems, e.g., electrolytes,<sup>2</sup> protein,<sup>3</sup> and micellar surfaces.<sup>4</sup>

In this work, we mainly used the acceptor-donor-hydrogen (ADH) criterion: two water molecules are H-bonded if their inter-oxygen distance  $r_{OO}$  is less than the cutoff radius<sup>5</sup>  $r_{OO}^c = 3.5$  (Å) and the H-O···O angle  $\phi$  is less than cutoff angle  $\phi^c = 30^\circ$ .<sup>6–9</sup> For comparison, we also used another definition of HB (AHD): when the distance between the O atoms of two water molecules is less than the cutoff radius  $r_{OO}^c$ , and the O-H···O included angle  $\theta$  is greater than cutoff angle  $\theta^c = 120^\circ$ , then we say that there is a HB between the two molecules.

We use a configuration  $r(t)$  to denote the positions of all the atoms in the system at time  $t$ . Either of the criteria above allows one to define an HB population  $h[r(t)] = h(t)$ , which equals 1 when a tagged pair of molecules are H-bonded, and 0 otherwise. The fluctuation in  $h(t)$  from its time-independent equilibrium average is defined by<sup>10</sup>  $\delta h = h(t) - \langle h \rangle$ . The probability that a specific tagged pair of molecules is H-bonded in a large system is extremely small<sup>1</sup>, then  $\delta h(t) = h(t)$ . Therefore, the correlation of  $\delta h(t)$  can be written as

$$\langle \delta h(0)\delta h(t) \rangle = \langle h(0)h(t) \rangle,$$

where the averaging  $\langle \dots \rangle$  is to be performed over the ensemble of initial conditions.

The correlation function  $c(t) = \langle h(0)h(t) \rangle / \langle h \rangle$  describes the structural relaxation of H-bonds.<sup>2,11</sup> Here the average  $\langle h \rangle$  of the HB population is the probability that a pair of randomly chosen water molecules in the system is H-bonded at any time  $t$ . The function  $c(t)$  measures correlation in  $h(t)$  independent of any possible bond-breaking events, and it relaxes to zero when  $t$  is large.<sup>12</sup>

Because the thermal motion can cause distortions of H-bonds from the perfectly tetrahedral configuration, water molecules show a librational motion on a time scale of  $\sim 0.1$  ps superimposed to rotational and diffusional motions ( $> 1$  ps), which causes a time variation in interaction parameters. A new HB population  $h^{(d)}(t)$  was also defined to obviate the distortion of real HB dynamics due to the above geometric definition.<sup>2,5</sup> It is 1 when the inter-oxygen distance of a particular tagged pair of water molecules is less than  $r_{\text{OO}}^c$  at time  $t$ , and 0 otherwise. The H-bonds between a tagged molecular pair that satisfy the condition  $h^{(d)}(t) = 1$  may have been broken, but they may more easily form H-bonds again. The correlation function

$$n(t) = \frac{\langle h(0)[1 - h(t)]h^{(d)}(t) \rangle}{\langle h \rangle} \quad (1)$$

---

<sup>1</sup>The average number of H-bonds in an equilibrium of  $N$  water molecules is:  $\frac{1}{2}N(N - 1)\langle h \rangle \sim N$ . It implies that  $\frac{1}{2}N\langle h \rangle \sim 1$ . For a large system,  $\langle h \rangle$  is extremely small.

represents the probability at time  $t$  that a tagged pair of initially H-bonded water molecules are unbonded but remain separated by less than  $r_{\text{OO}}^c$ .<sup>2</sup>

The rate of HB relaxation to equilibrium is characterized by the reactive flux<sup>13</sup>

$$k(t) = -\frac{dc(t)}{dt}, \quad (2)$$

which quantifies the rate that an initially present HB breaks at time  $t$ , independent of possible breaking and reforming events in the interval from 0 to  $t$ . Therefore,  $k(t)$  measures the effective decay rate of an the initial set of H-bonds.<sup>10</sup> For bulk water, a 0.2-ps transient period exists, during which  $k(t)$  changes quickly from its initial value.<sup>14</sup> However, at longer times,  $k(t)$  is independent of the HB definitions.

## 2 Hydrogen bond breaking and reforming rate constants

Assume that each HB acts independently of other H-bonds,<sup>1,13</sup> and due to the detailed balance condition, one obtains  $\tau_{\text{HB}} = (1 - \langle h \rangle)/k$ , where  $k$  is the rate constant of breaking an HB, i.e., the forward rate constant.<sup>15,16</sup> Correspondingly, the backward rate constant  $k'$  is represented by the rate constant from the HB-on state to the HB-off state for a tagged pair of molecules. Based on the functions  $n(t)$ ,  $h(t)$ ,  $h^{(\text{d})}(t)$ , and  $k(t)$ , Khalilullin and Kühne<sup>17</sup> have obtained the ratio  $k/k'$  of HB breaking and reforming rate constants in bulk water, and then the lifetime and relaxation time of H-bonds from simulations. Here, for the air-water interface, we obtain the optimal solution range of  $k$  and  $k'$  from the relationship between the reactive flux  $k(t)$  and the correlation functions  $c(t)$  and  $n(t)$ :

$$k(t) = kc(t) - k'n(t). \quad (3)$$

We obtain the optimal value of the rate constants,  $k$  and  $k'$ , by the least squares fit of  $k(t)$ ,  $c(t)$ , and  $n(t)$  beyond the transition phase. The function  $c(t)$  is regarded as a column vector composed of  $(c_1, \dots, c_P)^T$ , and is denoted as  $\mathbf{c}$ , with  $c_i$  representing the value of correlation  $c(t)$  at  $t = i$ . Similarly,  $n(t)$  and  $k(t)$  can also be denoted as  $\mathbf{n}$  and  $\mathbf{k}$ , respectively. Then, the rate constants  $k$  and  $k'$  are determined from the matrix  $\mathbf{A} = [\mathbf{c} \quad \mathbf{n}]$ :

$$\begin{bmatrix} k \\ -k' \end{bmatrix} = (\mathbf{A}^T \mathbf{A})^{-1} \mathbf{A}^T \mathbf{k}. \quad (4)$$

### 3 Details of Scenario 1: the Luzar-Chandler (LC) method

In Scenario 1, to obtain interface HB dynamics, we use molecule sampling at the instantaneous interface. Let  $T_e$  be the time it takes for all water molecules in the simulation box to traverse the interface and bulk phase, and  $\tau_{\text{HB}}$  be the characteristic time of HB dynamics.

If the trajectory length  $t_{\text{traj}}$  satisfies the condition  $\tau_{\text{HB}} \ll t_{\text{traj}} \ll T_e$ , we sample interfacial water molecules at time points  $t_p$  ( $p = 1, \dots, M$ ) that are evenly spaced on the trajectory, then obtain interface HB dynamics using the following procedure:

1. For each simulation time step, define a pair of interfaces with a thickness  $d$  as shown in Figure 1 in the main text. At each  $t_p$ , we select a set  $S_p$  of water molecules in the pair of interfacial layers  $\mathcal{I}(d; t)$ , i.e.,  $\mathbf{r}(t_p) \in \mathcal{I}(d; t_p)$ . The set of interfacial water molecules is given by the union of  $S_p$ . This sampling process of interface water can be seen in Figure S1. Then we calculate the correlation functions  $c(t)$ ,  $n(t)$ , and  $k(t)$  through  $t_{\text{traj}}$  for these water molecules belonging to the set  $S_p$  of interfacial water molecules.
2. Calculate average functions of the correlation functions  $c(t)$ ,  $n(t)$ , and  $k(t)$  respectively over all sub-trajectories.
3. Calculate reaction rate constants of breaking and reforming for the interfacial layer  $\mathcal{I}(d; t)$  by Equation 3.

In Scenario 1, the interfacial water-picking is performed every 4 ps.

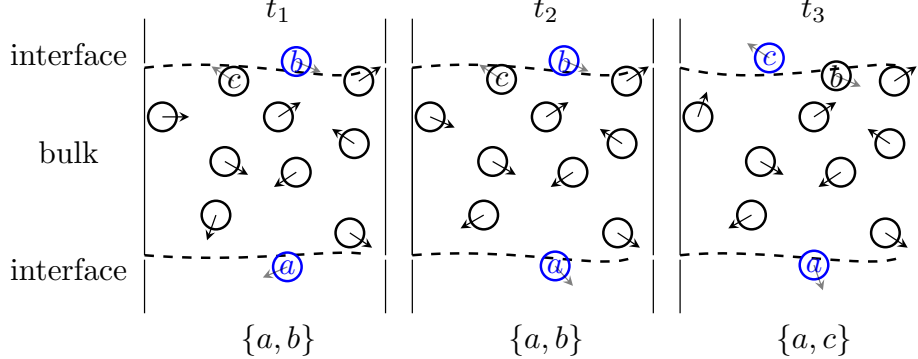


Figure S1: The sampling of water molecules at the interface in Scenario 1. The figure shows the configuration of the system at three water-picking moments. As a schematic diagram, we use circles to represent water molecules and dotted curves to represent the boundaries of the air-water interface. The three moments  $t_1$ ,  $t_2$ , and  $t_3$  belong to the same sub-trajectory. At these three moments, the interface water molecules (in blue) we selected are  $\{a, b\}$ ,  $\{a, b\}$  and  $\{a, c\}$ , respectively. Therefore, in this sub-trajectory, we use their union as the interface water molecules, that is,  $\{a, b, c\}$ .

## 4 Rotational anisotropy decay of OH stretch at the air-water interface

We examine the water interface thickness results from the interfacial HB dynamics by polarization anisotropy decay of OH stretch. The polarization anisotropy decay of the OH stretch can also provide information on the water dynamics.<sup>18–21</sup> We assume that the anisotropy decay  $R(t)$  is only due to the orientational relaxation of water molecules. Within the Condon approximation,<sup>22</sup> it is directly related to the orientational correlation function  $C_2(t)$ <sup>21,23–25</sup> through  $R(t) = \frac{2}{5}C_2(t)$ . The  $C_2(t)$  is given by the rotational time-correlation function

$$C_2(t) = \langle P_2(\hat{u}(0) \cdot \hat{u}(t)) \rangle, \quad (5)$$

where  $P_2(x)$  is the second-order Legendre polynomial,<sup>26</sup> i.e.,  $P_2(x) = \frac{1}{2}(3x^2 - 1)$ ,  $\hat{u}(t)$  is the time-dependent unit vector of the transition dipole, and  $\langle \rangle$  indicate equilibrium ensemble

average.<sup>27</sup> In our simulations, we concentrate on water molecules and consider a unit vector directed along the OH bond.

For the air-water interface, using the Method section in the main text, we obtain the instantaneous interface with thickness  $d = 1, \dots, 6$  ( $\text{\AA}$ ). Then, for each value of  $d$ , the LC method is used to obtain  $C_2(t)$  for water molecules at the air-water interface.

## 5 Computational Methods

### 5.1 Density functional theory-based molecular dynamics (DFTMD) simulations

To describe the subtleties of H-bonding in water,<sup>28</sup> we have performed DFTMD simulations<sup>29</sup> for bulk water and the air-water interface. The simulations make use of technologies that have been successfully tested on water and solutions,<sup>30–32</sup> namely the Goedecker-Teter-Hutter (GTH) pseudopotentials,<sup>33–35</sup> Generalised Gradient Approximation (GGA) of the exchange-correlation functional,<sup>36,37</sup> and dispersion force correction, DFT-D3.<sup>38,39</sup> By eliminating the strongly bound core electrons, the GTH pseudopotentials reduce the number of occupied electronic orbitals that have to be treated in an electronic structure calculation. There are dual-space Gaussian-type pseudopotentials that are separable and satisfy a quadratic scaling to system size.<sup>40</sup> The GGA functionals generally describe the dipole and quadrupole moments of the molecules quite well, and the DFT-D3 correction treats the van der Waals dispersion forces and improves the structural properties without more computational cost and thus can be used for the air-water interface.

The DFTMD calculation is implemented by an NVT code that is implemented in the CP2K/QUICKSTEP package.<sup>41,42</sup> The BLYP XC functional, which consists of Becke non-local exchange<sup>36</sup> and Lee-Yang-Parr correlation<sup>37</sup> has been employed. The electron-ion interactions are described by GTH pseudopotentials.<sup>34,43</sup> A Gaussian basis for the wave functions and an auxiliary plane wave basis set for the density is used in this scheme. The DZVP-GTH

basis set is used for all atoms and a cutoff of 280 (Ry) is chosen for the charge density.<sup>41</sup> The Nosé-Hoover chain thermostat<sup>44</sup> is used to conserve the temperature at 300 (K). The simulation for the air-water interface uses a time step of 0.5 (fs). The reference density for determining the instantaneous interface is set to 0.016 (g/cm<sup>3</sup>).

The bulk water system consisted of 128 water molecules in a periodic box of size 15.64 × 15.64 × 15.64 (Å<sup>3</sup>), and with a density of 1.00 (g/cm<sup>3</sup>). The slab consisted of 128 water molecules in a periodic box of size 15.64 × 15.64 × 31.28 (Å<sup>3</sup>). The length of each trajectory is 60 (ps).

## 5.2 Deep potential molecular dynamics (DeePMD) simulations

DeePMD simulations based on MB-pol<sup>45–48</sup> were conducted using LAMMPS<sup>49</sup> package for different sizes of air-water interfaces, ranging from 125 to 1000 water molecules. Initially, water molecules were placed in the middle of a simulation box in 3D periodic boundary conditions. The equations of motion were integrated using the velocity-Verlet algorithm with a time step of 0.5 (fs). The temperature was maintained at 300 (K) using a Nosé–Hoover thermostat with a time constant of 0.5 (ps). The system was simulated in the NVT ensemble, ensuring the constant number of particles, volume, and temperature throughout the simulation. Details of simulation settings for all systems are provided in Table S1.

Table S1: Number ( $N$ ) of water molecules, box dimensions ( $a$ ,  $b$ ,  $c$ ) along  $x$ ,  $y$  and  $z$  axes, temperature (Temp.) and surface tension  $\gamma$  values for different air-water interface systems.

	125	216	343	512	729	1000
$a$ (Å)	15.52	19.71	21.72	24.63	27.93	31.28
$b$ (Å)	15.52	19.71	21.72	24.63	27.93	31.28
$c$ (Å)	77.60	98.55	108.64	123.19	139.69	156.44
Temp. (K)	300	300	300	300	300	300
Time (ps)	842	775	300	705	300	300
$\gamma$ (mN/m)	68.93±3.48	71.53±3.80	70.23±3.48	69.60±2.60	70.72±4.10	70.09±4.96

### 5.3 Surface tension calculations

The surface tension  $\gamma$  is calculated from the pressure tensor by considering all the atoms in a system:

$$\gamma = \frac{L_z}{2} [\langle P_{zz} \rangle - 0.5 (\langle P_{xx} \rangle + \langle P_{yy} \rangle)] \quad (6)$$

where  $L_z$  is the box length in the z-dimension, and  $P_{ii}$  are the diagonal components of the pressure tensor. The factor 2 accounts for the two liquid-vapor interfaces in the system.<sup>50–52</sup> In practice, the pressure tensors are obtained from the thermodynamic log from LAMMPS.<sup>49</sup> For each non-overlapping 40 ps sub-trajectory along the entire trajectory, we conduct one measurement of surface tension through Equation 6. The sliding value of surface tension is then calculated across the whole trajectory. As shown in Figure S2, both sliding and accumulated surface tension values are plotted.

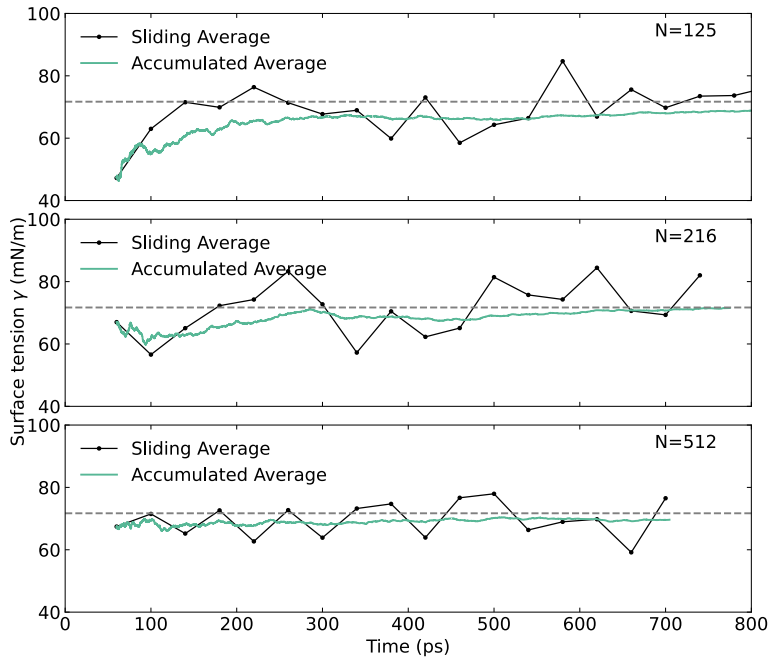


Figure S2: Time evolution of the sliding and accumulated surface tension values as computed by DeePMD simulations. The time length of a sub-trajectory used for one sliding average is 40 ps.

The surface tension value for each system is estimated from the sliding values, as detailed in Table S1 and Figure S11. It is worth noting that a sufficiently long simulation time is needed to obtain a stable surface tension value. The calculated surface tension values are consistent with the experimental value (71.70 mN/m).<sup>53</sup> Although long-range corrections are crucial for precise surface tension calculations, they were not included in our study due to its specific focus. These corrections are particularly important when precise quantification of surface tension is necessary.<sup>54,55</sup>

## 6 Results for verification

### 6.1 Results based on DFTMD simulations

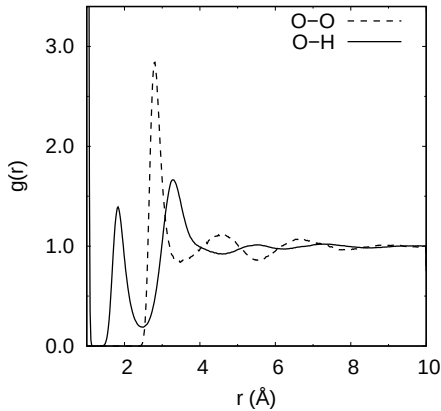


Figure S3: The partial radial distribution functions (RDFs) for the simulated bulk water.

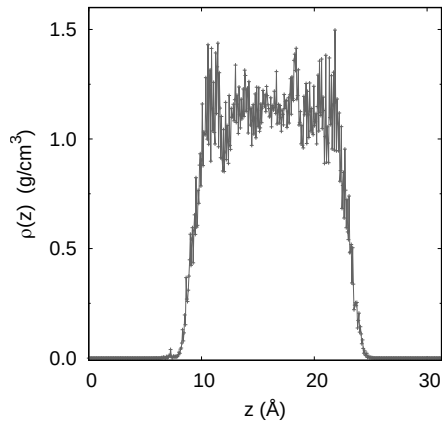


Figure S4: The density  $\rho(z)$  along the interface normal of the slabs of 128 water molecules, simulated by DFTMD simulations. It can be seen that in the middle part of the interface, the density of water is 1.0 g/cm<sup>3</sup>. This value is close to the density of the bulk water.

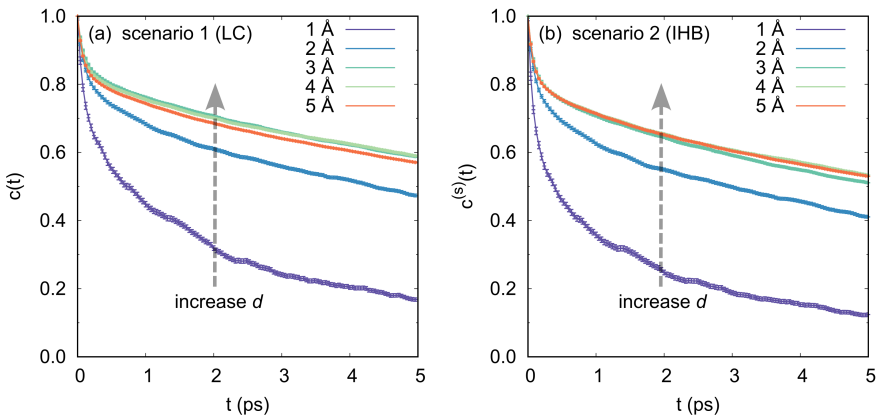


Figure S5: The  $c(t)$  and  $c^{(s)}(t)$  for interface H-bonds obtained from the ADH criterion ( $r_{OO}^c, \phi^c$ ) = (3.5 Å, 30°) of HB definition for (a) Scenario 1 (LC); (b) Scenario 2 (IHB). Two features can be found: (i). As  $d$  increases, both  $c(t)$  and  $c^{(s)}(t)$  eventually approach a stable function. (ii). The decay rate of  $c^{(s)}(t)$  in Scenario 2 surpasses  $c(t)$  in Scenario 1. This is visually represented by two dashed directed line segments, positioned identically to the graphs.

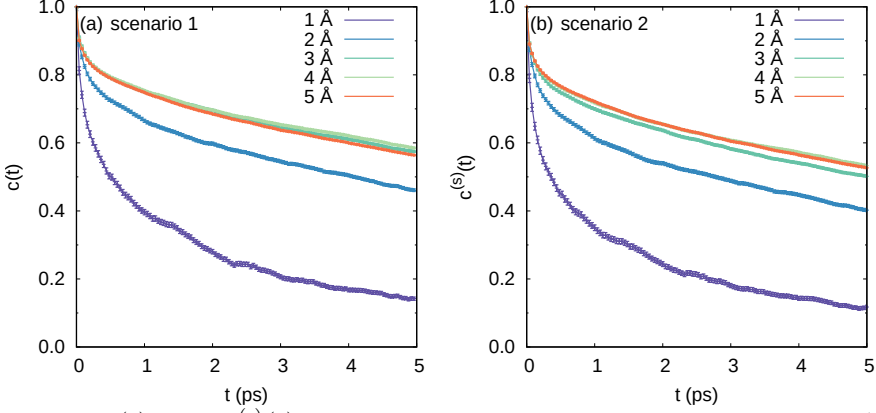


Figure S6: The  $c(t)$  and  $c^{(s)}(t)$  for interface H-bonds obtained from the AHD criterion ( $(r_{OO}^c, \theta^c) = (3.5 \text{ \AA}, 120^\circ)$ ) of HB definition for (a) Scenario 1 (LC); (b) Scenario 2 (IHB). Similar to the case of ADH, the same features can be found: (i). As  $d$  increases, both  $c(t)$  and  $c^{(s)}(t)$  eventually approach a stable function. (ii). The decay rate of  $c^{(s)}(t)$  in Scenario 2 surpasses  $c(t)$  in Scenario 1. As can be seen from Figures S5 and S6, the above two features do not particularly depend on the specific definition of H-bonds.

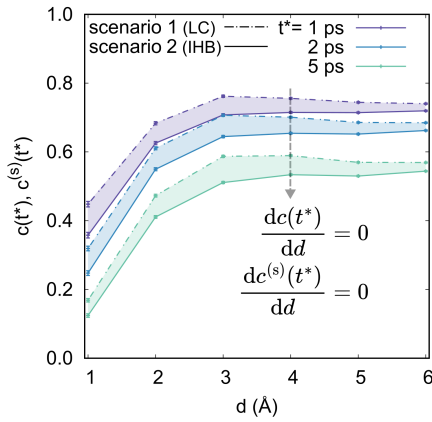


Figure S7: The  $d$ -dependence of the correlation functions at reference time points  $t^* = 1, 2, 5$  (ps), revealing key insights into the dynamics of the air-water interface: (i). As  $d$  increases, both  $c(t^*)$  and  $c^{(s)}(t^*)$  show an upward trend, with their rates of change gradually approaching 0. (ii). For each  $t^*$ ,  $c(t)$  is slightly larger than  $c^{(s)}(t)$  for the same  $d$ . (iii). The thickness  $d_f = 4$  (\text{\AA}) of the air-water interface is obtained from the  $d$ -dependence of  $c(t^*)$  and  $c^{(s)}(t^*)$ , obtained by the LC method (dot-dashed lines) and the IHB method (solid lines), respectively.

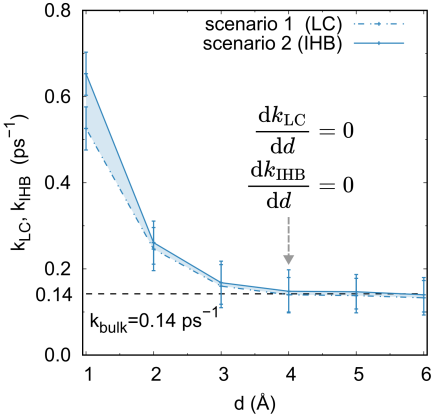


Figure S8: The breaking HB reaction rate constants  $k_{LC}$  and  $k_{IHB}$  obtained by the IHB method and the LC method, respectively. (i). Both constants,  $k_{LC}$  and  $k_{IHB}$ , decrease monotonically to the HB breaking rate  $k_{bulk}$  for the bulk water as  $d$  increases. (ii).  $k_{LC}$  is smaller than  $k_{IHB}$  for the same  $d$ . (iii). The thickness  $d'_f = 4$  (Å) of the air-water interface is obtained from the  $d$ -dependence of  $k_{IHB}$  and  $k_{LC}$ , respectively.

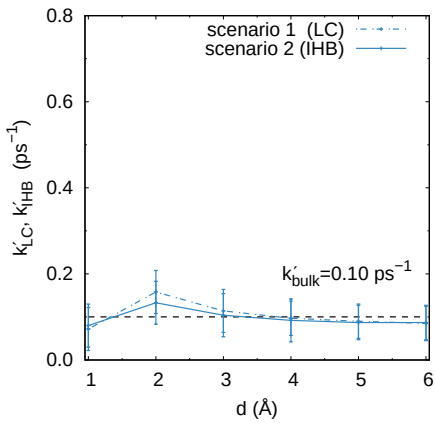


Figure S9: The  $d$ -dependence of the rate constant  $k'_{IHB}$  and  $k'_{LC}$ , obtained by the IHB (solid lines) and the Luzar-Chandler (dot-dashed lines) methods, respectively. The corresponding reaction rate  $k'_{bulk}$  for bulk water is also represented as dashed lines. The ADH criterion of H-bonds is used and the fits are carried on the time region  $0.2 < t < 12$  (ps).

For bulk water and the air-water interface, the  $k$  and  $k'$  are reported in Table S2 and S3.

Table S2: The  $k$  and  $k'$  for the bulk water and the air-water interface (the time region  $0.2 < t < 2$  (ps)).

Criterion	$k$ (b) <sup>2</sup>	$k'$ (b)	$\tau_{\text{HB}}$ (b) <sup>3</sup>	$k$ (i)	$k'$ (i)	$\tau_{\text{HB}}$ (i)
ADH	0.296	0.988	3.380	0.323	0.765	3.101
AHD	0.288	1.149	3.470	0.314	0.887	3.184

Table S3: The  $k$  and  $k'$  for the bulk water and the air-water interface (the time region  $2 < t < 12$  (ps)).

Criterion	$k$ (b)	$k'$ (b)	$\tau_{\text{HB}}$ (b)	$k$ (i)	$k'$ (i)	$\tau_{\text{HB}}$ (i)
ADH	0.115	0.039	8.718	0.157	0.068	6.372
AHD	0.105	0.047	9.496	0.155	0.088	6.472

## 6.2 Results based on DeePMD simulations

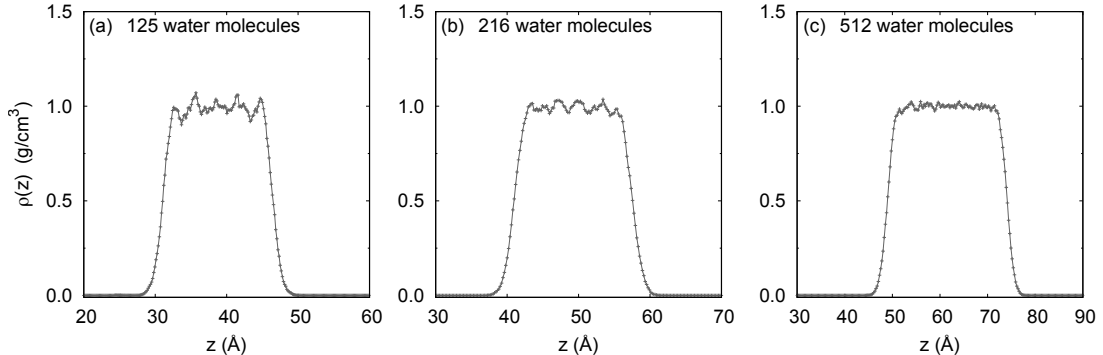


Figure S10: The Density  $\rho(z)$  along the interface normal of  $\text{H}_2\text{O}$  in the slabs of 125 (a), 216 (b), and 512 (c) water molecules, simulated by DeePMD simulations with MB-pol. The density values for these systems closely align well with the bulk water density,  $1.0 \text{ (g/cm}^3)$ .

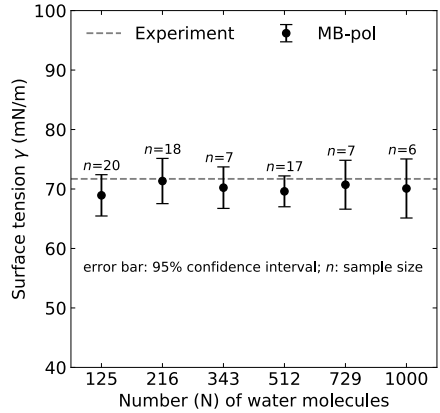


Figure S11: Surface tension  $\gamma$  for different size of systems. The surface tension values are consistent with the experimental value of 71.70 (mN/m) at 300 (K).<sup>53</sup> The error bars represent the 95% confidence interval, and sample size  $n$ , i.e., the number of non-overlapped 40 ps sub-trajectories, to calculate the error bar are shown in the figure.

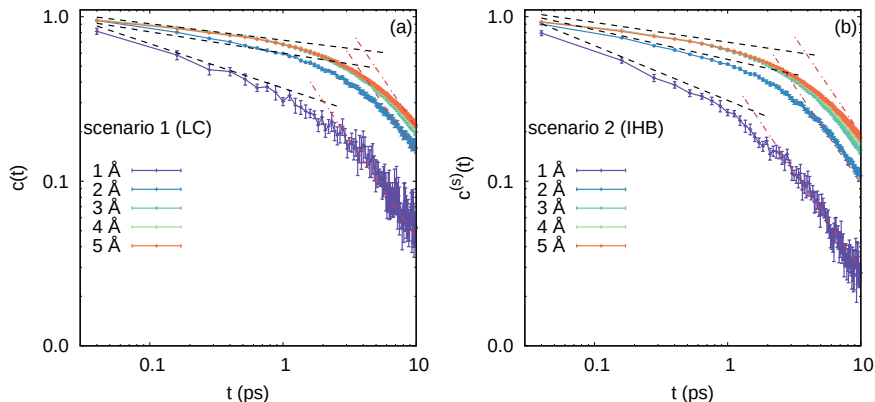


Figure S12: The auto-correlation functions for interface H-bonds with varying thickness  $d$  are displayed on a log-log scale for (a) Scenario 1 (LC) and (b) Scenario 2 (IHB). With a critical time  $t^c$  serving as the boundary, the decay of  $c(t)$  and  $c^{(s)}(t)$  can be characterized by two power-law phases: short-term decay and long-term decay. In the short-term phase, both  $c(t)$  and  $c^{(s)}(t)$  follow a  $t^{-\alpha_1}$  law, with the exponent  $\alpha_1$  decreasing from 0.3 to 0.1 as  $d$  increases from 1 to 5 ( $\text{\AA}$ ). The long-term decay follows a  $t^{-\alpha_2}$  law with an exponent  $\alpha_2 \approx 1.2$  for all thicknesses. For both scenarios,  $t^c \approx 2$  (ps) for  $d = 1$  ( $\text{\AA}$ ), and  $t^c$  increases with the increase of  $d$ .

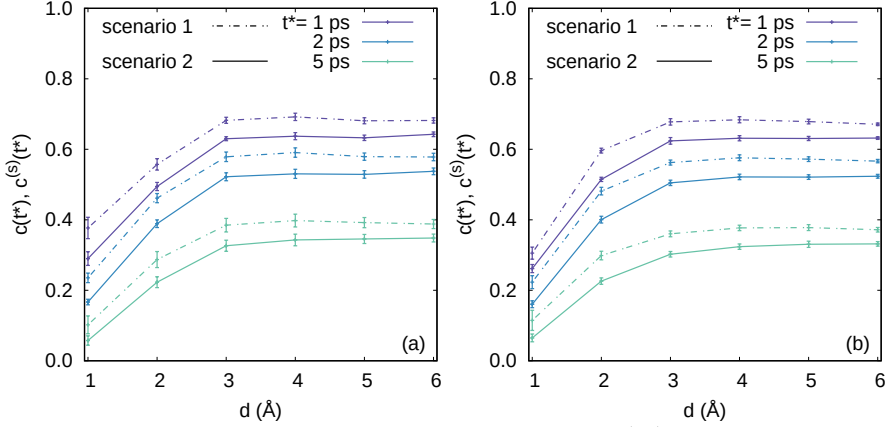


Figure S13: The  $d$ -dependence of the correlation function  $c(t^*)$  at three reference time points  $t^* = 1, 2, 5$  (ps), revealing key insights into the dynamics of two air-water interface models, simulated by DeePMD with MB-pol: (a) 125 water molecules; (b) 216 water molecules. Similar to the results of the interface model of 512 water molecules. (i). As  $d$  increases, both  $c(t^*)$  and  $c^{(s)}(t^*)$  show an upward trend, with their rates of change gradually approaching 0. (ii). For each  $t^*$ ,  $c(t)$  is slightly larger than  $c^{(s)}(t)$  for the same  $d$ . (iii). The thickness  $d_f = 4$  ( $\text{\AA}$ ) of the air-waterinterface is obtained from the  $d$ -dependence of  $c(t^*)$  and  $c^{(s)}(t^*)$ , obtained by the LC method (dot-dashed lines) and the IHB method (solid lines).

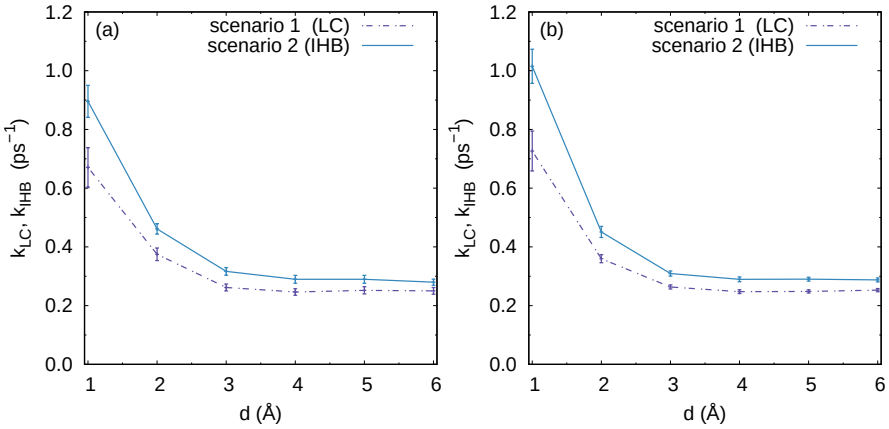


Figure S14: The breaking HB reaction rate constants  $k_{\text{LC}}$  and  $k_{\text{IHB}}$  obtained by the LC and IHB methods respectively: (a) 125 water molecules; (b) 216 water molecules.

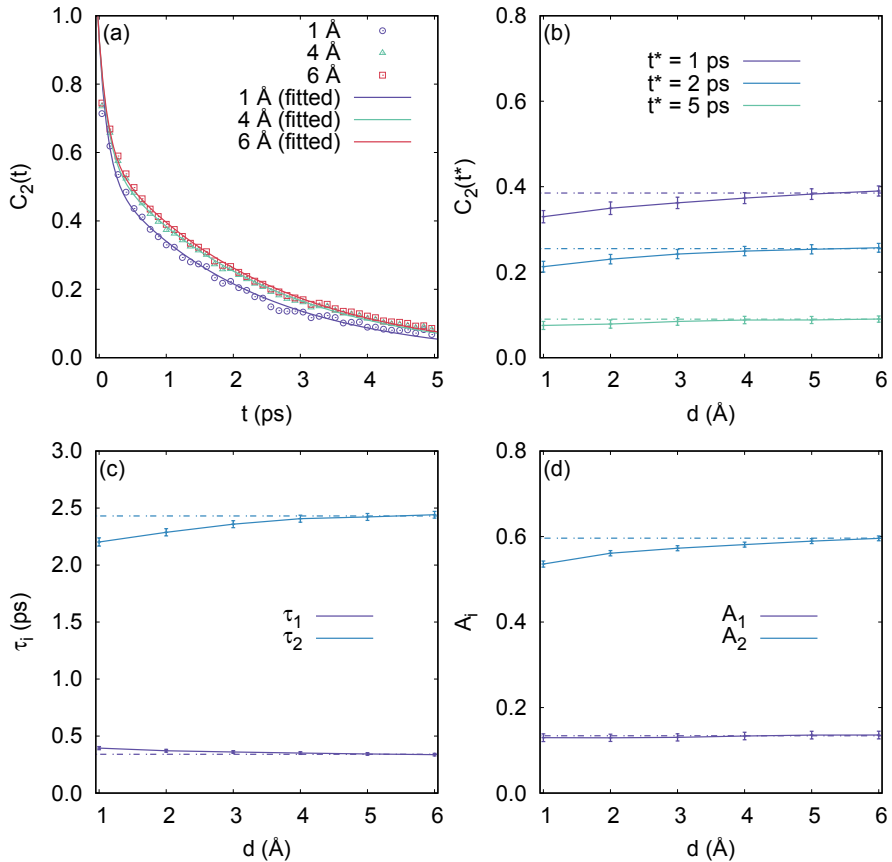


Figure S15: The orientation correlation function  $C_2(t)$  for the air-water interface simulated with 125 water molecules. (a) The  $C_2(t)$  for  $d = 1, 4, 6$  Å and the bi-exponential fitted functions  $C_2(t) = A_1 \exp(t/\tau_1) + A_2 \exp(t/\tau_2)$ . The  $d$ -dependence of (b)  $C_2(t^*)$  for water molecules at the air-water interface with  $t^* = 1, 2, 5$  (ps) and (c) relaxation time ( $\tau_1$  and  $\tau_2$ ), and (d) the amplitude ( $A_1$  and  $A_2$ ). The dotted lines are horizontal to enhance visibility (this applies to Figure S16 as well).

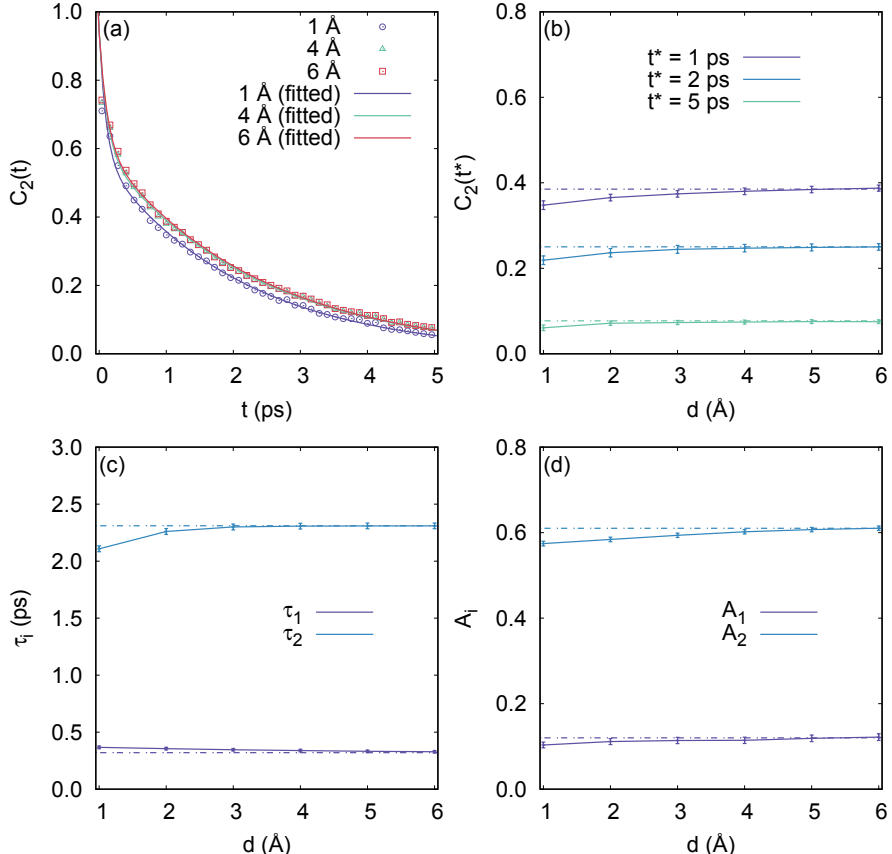


Figure S16: The orientation correlation function  $C_2(t)$  for the air-water interface simulated with 216 water molecules. (a) The  $C_2(t)$  for  $d = 1, 4, 6$  ( $\text{\AA}$ ) and the bi-exponential fitted functions  $C_2(t) = A_1 \exp(t/\tau_1) + A_2 \exp(t/\tau_2)$ . The  $d$ -dependence of (b)  $C_2(t^*)$  for water molecules at the air-water interface with  $t^* = 1, 2, 5$  (ps) and (c) relaxation time ( $\tau_1$  and  $\tau_2$ ), and (d) the amplitude  $A_1$  and  $A_2$ . From the convergence trend of  $\tau_1$  and  $\tau_2$  in (c), we find that the OH orientation relaxation of the air-water interface no longer changes at the interface with a thickness greater than 4 ( $\text{\AA}$ ). From Figure S15 and this figure, as  $d$  increases to 4 ( $\text{\AA}$ ),  $C_2(t^*)$  and  $\tau_i$ ,  $A_i$  all converge to a fixed value, respectively. The results are consistent with the results of Figure 5 and with the conclusion that the air-water interface thickness is 4 ( $\text{\AA}$ ) given by the interfacial HB dynamics.

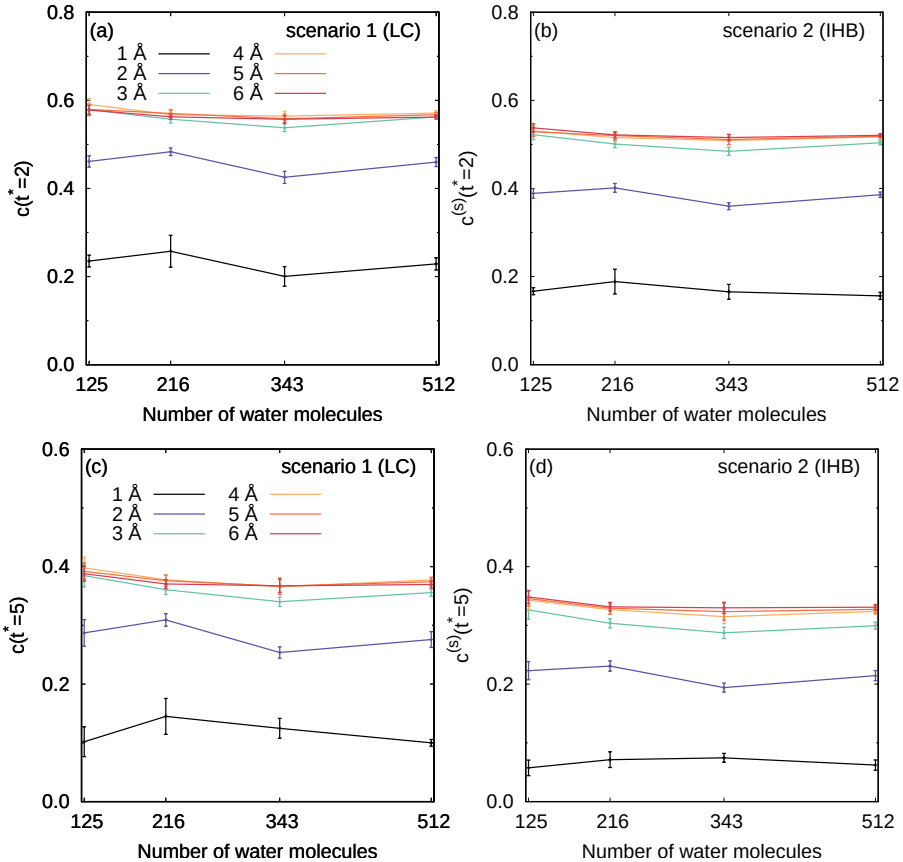


Figure S17: The system size-dependence of HB population correlation functions for the air-water interface at reference time  $t^*$  in two scenarios respectively: (a–b)  $t^* = 2$  (ps); (c–d)  $t^* = 5$  (ps). For small  $d$ ,  $c(t^*)$  ( $c^{(s)}(t^*)$ ) fluctuates slightly with the number ( $N$ ) of molecules, and its standard error gradually decreases. For  $d \geq 4$  (Å), their values do not dependent on  $N$  when  $N \geq 216$ .

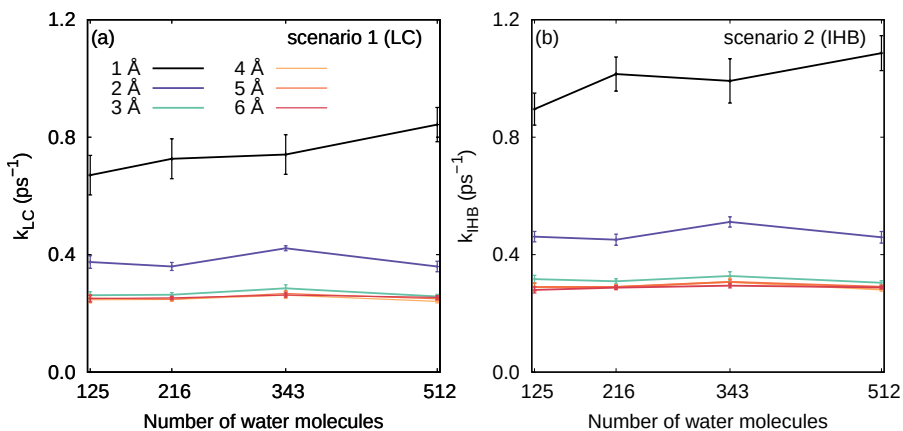


Figure S18: The system size-dependence of the (a)  $k_{LC}$  and (b)  $k_{IHB}$  for the air-water interface. There are fluctuations when  $d \leq 2$  ( $\text{\AA}$ ), and there is a slight trend of increasing with the increase of  $N$ . However, when  $d \geq 4$  ( $\text{\AA}$ ), the  $N$ -dependence of the reaction constant is not obvious.

### 6.3 Perspectives Derived from the Correlation Function of Free OH Groups

Similar to the interfacial HB dynamics, we also determine the thickness of the air-water interface from the perspective of free OH groups. Based on the definition of the free OH group defined in Reference 56, we define *interfacial* free OH group population  $n_f^{(s)}$  at the air-water interface as

$$n_f^{(s)}[\mathbf{r}(t)] = \begin{cases} 1 & \mathbf{r}_i \in \mathcal{I}(d; t), \\ & i \text{ is not H-bonded;} \\ 0 & \text{otherwise} \end{cases} \quad (7)$$

where  $\mathbf{r}(t)$  is the configuration of the system at time  $t$ ,  $\mathbf{r}_i$  is the position coordinate of the oxygen atom in an OH group, and  $\mathcal{I}(d; t)$  is the instantaneous interface layer with thickness  $d$  at time  $t$ . To test our previous results further, the auto-correlation function

$$c_f^{(s)}(t) = \frac{\langle n_f^{(s)}(0)n_f^{(s)}(t) \rangle}{\langle n_f^{(s)} \rangle} \quad (8)$$

for the interfacial free OH group population based on both  $R\text{-}\beta$  and  $R\text{-}\theta$  definition<sup>56</sup> of HB are calculated. In the calculation of this correlation function, the optimized geometry-based definitions for the free OH groups are given by  $(R_c, \beta_c) = (3.5 \text{ \AA}, 50^\circ)$  and  $(R_c, \theta_c) = (3.5 \text{ \AA}, 110^\circ)$ , respectively.<sup>56</sup> The correlation for the air-water interface based on two definitions of HB are shown in Figure S19a-b, respectively. It can be seen that, with a critical time  $t_c \approx 1.7$  (ps) (marked by black arrows in Figure S19a-b) as the boundary, there is a significant difference in the dependence of  $c_f^{(s)}(t)$  on the depth  $d$ : when  $t < t_c$ , the larger  $d$  is, the faster the relaxation of  $c_f^{(s)}(t)$  is; when  $t > t_c$ , the opposite is true. These results imply that these free OH groups close to the bulk phase appear to be freer than they are on the interface in a short time. However, from a longer time scale, their movement is not as fast as that on the interface. Despite the above differences, whether  $t < t_c$  or  $t > t_c$ , the rate of

change of the correlation function  $c_f^{(s)}(t)$  with  $d$  is basically equal to 0 when  $d = 5$  ( $\text{\AA}$ ) This conclusion can be seen from the slope  $d[c_f^{(s)}(t^*)]/dd$  for different reference time  $t^*$  as shown in Figure S19c.

Based on the correlation function  $c_f^{(s)}(t^*)$  at reference time  $t^* = 1, 2, 5$  (ps), we conclude that the air-water interface thickness  $d_f \approx 5$  ( $\text{\AA}$ ) is confirmed from the  $d$ -dependence of  $c_f^{(s)}(t^*)$  in both  $R\text{-}\beta$  and  $R\text{-}\theta$  definitions of HB, respectively.

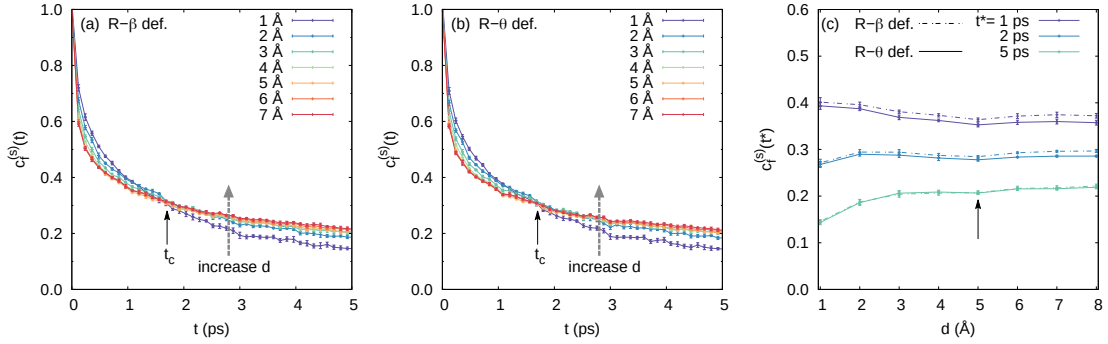


Figure S19: The free OH group correlation functions for the air-water interface simulated with 512 water molecules. The number  $N_s$  of samples is 6. (a-b)The time-dependence of the correlations  $c_f^{(s)}(t)$ . The definition of the free OH group is based on the optimized  $R\text{-}\beta$  and  $R\text{-}\theta$  definition of HB,<sup>56</sup> respectively. (c) The  $d$ -dependence of the correlation function  $c_f^{(s)}(t^*)$  at three reference time points  $t^* = 1, 2, 5$  (ps). The approximate value of  $d_f$  is marked by a black arrow. (Consistent results for systems with 125 and 216 water molecules are shown in Figures S20 and S21.)

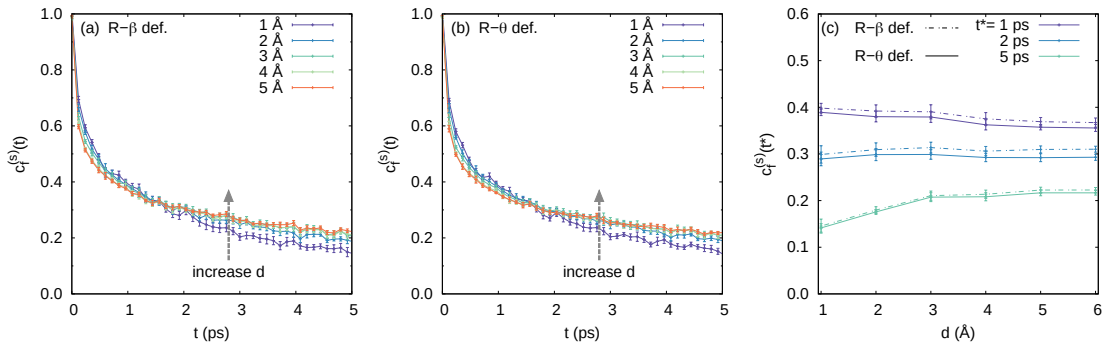


Figure S20: (a-b)The time-dependence of the correlation functions  $c_f^{(s)}(t)$  for air-water interface simulated with 125 water molecules. The definition of the free OH group is based on (a)  $R\text{-}\beta$  and (b)  $R\text{-}\theta$  definition of HB,<sup>56</sup> respectively. (c) The  $d$ -dependence of the correlation function  $c_f^{(s)}(t^*)$  at three reference time points  $t^* = 1, 2, 5$  (ps).

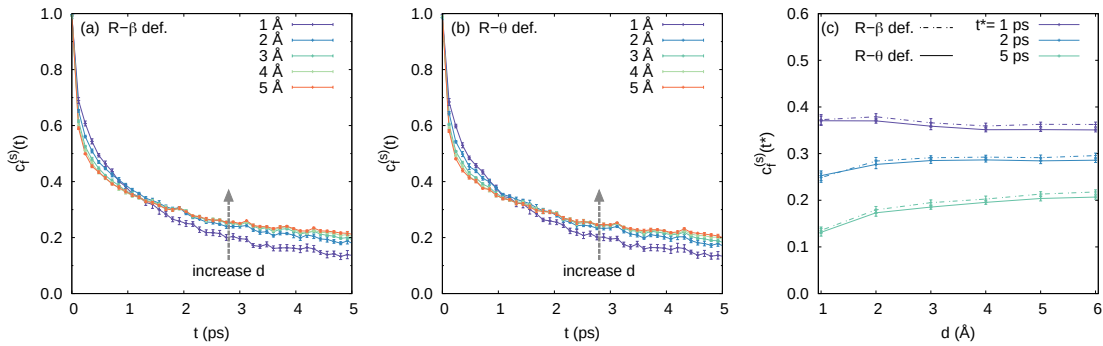


Figure S21: (a-b)The time-dependence of the correlations  $c_f^{(s)}(t) = \langle n_f^{(s)}(0)n_f^{(s)}(t) \rangle / \langle n_f^{(s)} \rangle$  for air-water interface simulated with 216 water molecules. The definition of the free OH group is the same as Figure S20. (c) The  $d$ -dependence of the correlation function  $c_f^{(s)}(t^*)$  at three reference time points  $t^* = 1, 2, 5$  (ps).

## References

- (1) Luzar, A.; Chandler, D. Effect of Environment on Hydrogen Bond Dynamics in Liquid Water. *Phys. Rev. Lett.* **1996**, *76*, 928–931.
- (2) Chandra, A. Effects of Ion Atmosphere on Hydrogen-Bond Dynamics in Aqueous Electrolyte Solutions. *Phys. Rev. Lett.* **2000**, *85*, 768–771.
- (3) Tarek, M.; Tobias, D. J. Role of protein-water hydrogen bond dynamics in the protein dynamical transition. *Phys. Rev. Lett.* **2002**, *88*, 138101.
- (4) Pal, S.; Bagchi, B.; Balasubramanian, S. Hydration Layer of a Cationic Micelle, C10TAB: Structure, Rigidity, Slow Reorientation, Hydrogen Bond Lifetime, and Solvation Dynamics. *J. Phys. Chem. B* **2005**, *109*, 12879–12890.
- (5) Sciortino, F.; Fornili, S. L. Hydrogen Bond Cooperativity in Simulated Water: Time Dependence Analysis of Pair Interactions. *J. Chem. Phys.* **1989**, *90*, 2786–2792.
- (6) Soper, A. K.; Phillips, M. G. A New Determination of the Structure of Water at 25 °C. *Chem. Phys.* **1986**, *107*, 47–60.

- (7) Teixeira, J.; Bellisent-Funel, M. C.; Chen, S. H. Dynamics of Water Studied by Neutron Scattering. *J. Phys. Condens. Matter* **1990**, *2*, SA105.
- (8) Luzar, A.; Chandler, D. Structure and hydrogen bond dynamics of water-dimethyl sulfoxide mixtures by computer simulations. *J. Chem. Phys.* **1993**, *98*, 8160–8173.
- (9) Balasubramanian, S.; Pal, S.; Bagchi, B. Hydrogen-Bond Dynamics Near a Micellar Surface: Origin of the Universal Slow Relaxation at Complex Aqueous Interfaces. *Phys. Rev. Lett.* **2002**, *89*, 115505.
- (10) Chandler, D. *Introduction to Modern Statistical Mechanics*; Oxford University press, Oxford, 1987.
- (11) Benjamin, I. Hydrogen Bond Dynamics at Water/Organic Liquid Interfaces. *J. Phys. Chem. B* **2005**, *109*, 13711–13715.
- (12) Rapaport, D. C. Hydrogen Bonds in Water: Network Organization and Lifetimes. *Mol. Phys.* **1983**, *50*, 1151–1162.
- (13) Luzar, A. Resolving the Hydrogen Bond Dynamics Conundrum. *J. Chem. Phys.* **2000**, *113*, 10663.
- (14) Starr, F. W.; Nielsen, J. K.; Sta, H. E. Hydrogen-Bond Dynamics for the Extended Simple Point-Charge Model of Water. *Phys. Rev. E* **2000**, *62*, 579–587.
- (15) Chandler, D. Roles of Classical Dynamics and Quantum Dynamics on Activated Processes Occurring in Liquids. *J. Stat. Phys.* **1986**, *42*, 49–67.
- (16) Chandler, D. Statistical Mechanics of Isomerization Dynamics in Liquids and the Transition State Approximation. *J. Chem. Phys.* **1978**, *68*, 2959–2970.
- (17) Khaliullin, R. Z.; Kühne, T. D. Microscopic Properties of Liquid Water from Combined Ab Initio Molecular Dynamics and Energy Decomposition Studies. *Phys. Chem. Chem. Phys.* **2013**, *15*, 15746–15766.

- (18) Woutersen, S.; Bakker, H. J. Resonant intermolecular transfer of vibrational energy in liquid water. *Nature* **1999**, *402*, 1.
- (19) Cowan, M. L.; Bruner, B. D.; Huse, N.; Dwyer, J. R.; Chugh, B.; Nibbering, E. T. J.; Elsaesser, T.; Miller, R. J. D. Ultrafast memory loss and energy redistribution in the hydrogen bond network of liquid H<sub>2</sub>O. *Nature* **2005**, *434*, 199.
- (20) Kraemer, D.; Cowan, M. L.; Paarmann, A.; Huse, N.; Nibbering, E. T. J.; Elsaesser, T.; Miller, R. J. D. Temperature dependence of the two-dimensional infrared spectrum of liquid H<sub>2</sub>O. *Proc. Natl. Acad. Sci. USA* **2008**, *105*, 437–442.
- (21) Yagasaki, T.; Ono, J.; Saito, S. Ultrafast energy relaxation and anisotropy decay of the librational motion in liquid water: A molecular dynamics study. *J. Chem. Phys.* **2009**, *131*, 164511.
- (22) Schmidt, J. R.; Corcelli, S. A.; Skinner, J. L. Pronounced Non-Condon Effects in the Ultrafast Infrared Spectroscopy of Water. *J. Chem. Phys.* **2005**, *123*, 044513.
- (23) Tokmakoff, A. Orientational correlation functions and polarization selectivity for non-linear spectroscopy of isotropic media. I. Third order. *J. Chem. Phys.* **1996**, *105*, 1–12.
- (24) Rezus, Y. L. A.; Bakker, H. J. Orientational dynamics of isotopically diluted H<sub>2</sub>O and D<sub>2</sub>O. *J. Chem. Phys.* **2006**, *125*, 144512.
- (25) Bakker, H.; Skinner, J. L. Vibrational Spectroscopy as a Probe of Structure and Dynamics in Liquid Water. *Chem. Rev.* **2010**, *110*, 1498.
- (26) Geiger, A.; Mausbach, P.; Schnitker, J.; Blumberg, R. L.; Stanley, H. E. Structure and Dynamics of the Hydrogen Bond Network in Water by Computer Simulations. *J. Phys. (Paris)* **1984**, *45*, C7–13–C7–30.
- (27) Lin, Y. S.; Pieniazek, P. A.; Yang, M.; Skinner, J. L. On the Calculation of Rotational

- Anisotropy Decay, as Measured by Ultrafast Polarization-Resolved Vibrational Pump-Probe Experiments. *J. Chem. Phys.* **2010**, *132*, 174505.
- (28) Laasonen, K.; Sprik, M.; Parrinello, M.; Car, R. "Ab initio" liquid water. *J. Chem. Phys.* **1993**, *99*, 9080–9089.
- (29) Marx, D.; Hutter, J. Ab Initio Molecular Dynamics: Theory and Implementation. *Modern Methods and Algorithms of Quantum Chemistry, J.Grotendorst (Ed.) John von Neumann Institute for Computing, Jülich, NIC Series* **2000**, *1*, 301–499.
- (30) Khatib, R.; Backus, E. H. G.; Bonn, M.; Perez-Haro, M.; Gaigeot, M.-P.; Sulpizi, M. Water Orientation and Hydrogen-Bond Structure at the Fluorite/Water Interface. *Sci. Rep.* **2016**, *6*, 24287.
- (31) Khatib, R.; Hasegawa, T.; Sulpizi, M.; Backus, E. H. G.; Bonn, M.; Nagata, Y. Molecular Dynamics Simulations of SFG Librational Modes Spectra of Water at the Water-Air Interface. *J. Phys. Chem. C* **2016**, *120*, 18665–18673.
- (32) Khatib, R.; Sulpizi, M. Sum Frequency Generation Spectra from Velocity-Velocity Correlation Functions. *J. Phys. Chem. Lett.* **2017**, *8*, 1310–1314.
- (33) Goedecker, S.; Teter, M.; Hutter, J. Separable Dual-Space Gaussian Pseudopotentials. *Phys. Rev. B* **1996**, *54*, 1703–1710.
- (34) Hartwigsen, C.; Goedecker, S.; Hutter, J. Relativistic separable dual-space Gaussian pseudopotentials from H to Rn. *Phys. Rev. B* **1998**, *58*, 3641–3662.
- (35) Krack, M. Pseudopotentials for H to Kr optimized for gradient-corrected exchange-correlation functionals. *Theor. Chem. Acc.* **2005**, *114*, 145–152.
- (36) Becke, A. D. Density-Functional Exchange-Energy Approximation with Correct Asymptotic Behavior. *Phys. Rev. A* **1988**, *38*, 3098.

- (37) Lee, C.; Yang, W.; Parr, R. G. Development of the Colic-Salvetti Correlation-Energy Formula into a Functional of the Electron Density. *Phys. Rev. B* **1988**, *37*, 785.
- (38) Grimme, S.; Antony, J.; Ehrlich, S.; Krieg, H. A Consistent and Accurate Ab Initio Parametrization of Density Functional Dispersion Correction (DFT-D) for the 94 Elements H-Pu. *J. Chem. Phys.* **2010**, *132*, 154104.
- (39) Klimeš, J.; Michaelides, A. Perspective: Advances and Challenges in Treating van der Waals Dispersion Forces in Density Functional Theory. *J. Chem. Phys.* **2012**, *137*, 120901–120912.
- (40) Lu, J.-B.; Cantu, D. C.; Nguyen, M.-T.; Li, J.; Glezakou, V.-A.; Rousseau, R. Norm-Conserving Pseudopotentials and Basis Sets To Explore Lanthanide Chemistry in Complex Environments. *J. Chem. Theory Comput.* **2019**, *15*, 5987–5997.
- (41) VandeVondele, J.; Krack, M.; Mohamed, F.; Parrinello, M.; Chassaing, T.; Hutter, J. Quickstep: Fast and Accurate Density Functional Calculations using a Mixed Gaussian and Plane Waves Approach. *Comput. Phys. Commun.* **2005**, *167*, 103–128.
- (42) Kühne, T. D.; Iannuzzi, M.; Del Ben, M.; Rybkin, V. V.; Seewald, P.; Stein, F.; Laino, T.; Khaliullin, R. Z.; Schütt, O.; Schiffmann, F.; Golze, D.; Wilhelm, J.; Chulkov, S.; Bani-Hashemian, M. H.; Weber, V.; Borštník, U.; Taillefumier, M.; Jakobovits, A. S.; Lazzaro, A.; Pabst, H.; Müller, T.; Schade, R.; Guidon, M.; Andermatt, S.; Holmberg, N.; Schenter, G. K.; Hehn, A.; Bussy, A.; Belleflamme, F.; Tabacchi, G.; Glöß, A.; Lass, M.; Bethune, I.; Mundy, C. J.; Plessl, C.; Watkins, M.; VandeVondele, J.; Krack, M.; Hutter, J. CP2K: An electronic structure and molecular dynamics software package - Quickstep: Efficient and accurate electronic structure calculations. *J. Chem. Phys.* **2020**, *152*, 194103.
- (43) Lippert, G.; Hutter, J.; Parrinello, M. The Gaussian and Augmented-Plane-Wave Den-

- sity Functional Method for Ab Initio Molecular Dynamics Simulations. *Theor. Chem. Acc.* **1999**, *103*, 124.
- (44) Martyna, G. J.; Klein, M. L.; Tuckerman, M. Nosé-Hoover Chains: The Canonical Ensemble via Continuous Dynamics. *J. Chem. Phys.* **1992**, *97*, 2635.
- (45) Babin, V.; Leforestier, C.; Paesani, F. Development of a “First Principles” Water Potential with Flexible Monomers: Dimer Potential Energy Surface, VRT Spectrum, and Second Virial Coefficient. *J. Chem. Theory Comput.* **2013**, *9*, 5395–5403.
- (46) Babin, V.; Medders, G. R.; Paesani, F. Development of a “First Principles” Water Potential with Flexible Monomers. II: Trimer Potential Energy Surface, Third Virial Coefficient, and Small Clusters. *J. Chem. Theory Comput.* **2014**, *10*, 1599–1607.
- (47) Medders, G. R.; Babin, V.; Paesani, F. Development of a “First-Principles” Water Potential with Flexible Monomers. III. Liquid Phase Properties. *J. Chem. Theory Comput.* **2014**, *10*, 2906–2910.
- (48) Bore, S. L.; Paesani, F. Realistic phase diagram of water from “first principles” data-driven quantum simulations. *Nat. Commun.* **2023**, *14*.
- (49) Thompson, A. P.; Aktulga, H. M.; Berger, R.; Bolintineanu, D. S.; Brown, W. M.; Crozier, P. S.; in ’t Veld, P. J.; Kohlmeyer, A.; Moore, S. G.; Nguyen, T. D.; Shan, R.; Stevens, M. J.; Tranchida, J.; Trott, C.; Plimpton, S. J. LAMMPS - a flexible simulation tool for particle-based materials modeling at the atomic, meso, and continuum scales. *Comput. Phys. Commun.* **2022**, *271*, 108171.
- (50) Alejandre, J.; Tildesley, D. J.; Chapela, G. A. Molecular dynamics simulation of the orthobaric densities and surface tension of water. *J. Chem. Phys.* **1995**, *102*, 4574–4583.
- (51) Reddy, S. K.; Straight, S. C.; Bajaj, P.; Huy Pham, C.; Riera, M.; Moberg, D. R.; Morales, M. A.; Knight, C.; Götz, A. W.; Paesani, F. On the accuracy of the MB-

pol many-body potential for water: Interaction energies, vibrational frequencies, and classical thermodynamic and dynamical properties from clusters to liquid water and ice. *J. Chem. Phys.* **2016**, *145*, 194504.

- (52) Muniz, M. C.; Gartner, I., Thomas E.; Riera, M.; Knight, C.; Yue, S.; Paesani, F.; Panagiotopoulos, A. Z. Vapor–liquid equilibrium of water with the MB-pol many-body potential. *J. Chem. Phys.* **2021**, *154*, 211103.
- (53) Vargaftik, N. B.; Volkov, B. N.; Voljak, L. D. International Tables of the Surface Tension of Water. *J. Phys. Chem. Ref. Data.* **1983**, *12*, 817–820.
- (54) Nagata, Y.; Ohto, T.; Bonn, M.; Kühne, T. D. Surface tension of ab initio liquid water at the water-air interface. *J. Chem. Phys.* **2016**, *144*, 204705.
- (55) Muller, E. A.; Ervik, ; Mejía, A. A Guide to Computing Interfacial Properties of Fluids from Molecular Simulations [Article v1.0]. *LiveCoMS* **2020**, *2*.
- (56) Tang, F.; Ohto, T.; Hasegawa, T.; Xie, W. J.; Xu, L.; Bonn, M.; Nagata, Y. Definition of Free O–H Groups of Water at the Air–Water Interface. *J. Chem. Theory Comput.* **2017**, *14*, 357–364.